Nano Research

Open Access

Research Article

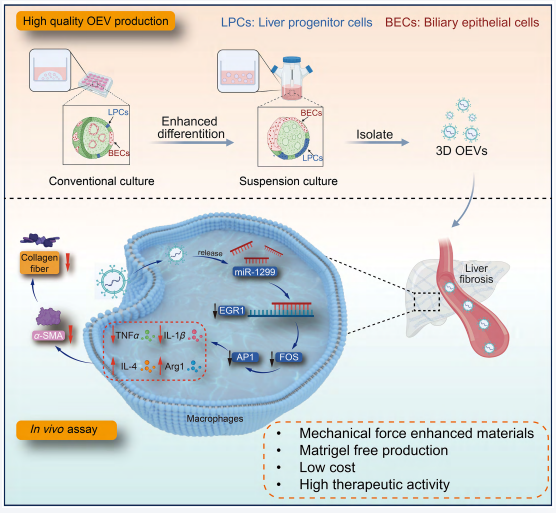
Development of multi-lineage differentiated liver ductal organoids in suspension culture that generates therapeutic extracellular vesicles for sclerosing cholangitis treatment

Senyi Gong[1,§], Yu Liu[1,§], Xingyu Luo[2], Yuwen Hu[1], Qinbiao Yan[1,3], Zhe Yang[2,4,5] ✉, Shusen Zheng[2,5] ✉, Meijin Guo[1] ✉, and Ali Mohsin[1] ✉

[1] *State Key Laboratory of Bioreactor Engineering, East China University of Science and Technology, Shanghai 200237, China*
[2] *Department of Hepatobiliary and Pancreatic Surgery, Key Laboratory of Artificial Organs and Computational Medicine in Zhejiang Province, Shulan (Hangzhou) Hospital, Shulan International Medical College, Zhejiang Shuren University, Hangzhou 310022, China*
[3] *Theseus Biotechnology (Shanghai) Company, Shanghai 200120, China*
[4] *Department of Hepatobiliary and Pancreatic Surgery, Shulan (Boao) Hospital, Boao 571434, China*
[5] *State Key Laboratory for Diagnosis and Treatment of Infectious Diseases, National Clinical Research Center for Infectious Diseases, National Medical Center for Infectious Diseases, Collaborative Innovation Center for Diagnosis and Treatment of Infectious Diseases, The First Affiliated Hospital, Zhejiang University School of Medicine, Hangzhou 310058, China*
§ *Senyi Gong and Yu Liu contributed equally to this work.*

Cite this article: *Nano Research*, **2026**, *19*, 94908921. https://doi.org/10.26599/NR.2026.94908921

ABSTRACT: Organoid-based therapy, as an approach in regenerative medicine, offers new options for previously untreatable diseases. However, the limitations of organoid transplantation, such as immunogenicity, tumorigenic potential, and ethical issues, restrict its clinical translation. For the first time, a novel three-dimension matrigel-free suspension culture system is developed to generate liver ductal organoid-derived extracellular vesicles (3D OEVs) for primary sclerosing cholangitis (PSC) treatment. The results show that the developed suspension culture provides a more favorable mechanical microenvironment, which significantly enhances the functional maturation of liver ductal organoids and their extracellular vesicles. This improvement is facilitated by a multidimensional regulatory network that encompasses the PI3K-AKT and RAP1 pathways. Moreover, 3D OEVs significantly attenuate hepatic inflammation and fibrosis because they can remodel the immune microenvironment, polarizing more macrophages into the anti-inflammatory M2 phenotypic macrophages. Furthermore, miR-1299 enriched in 3D OEVs is identified as the core effector molecule for macrophage reprogramming, which was confirmed by both *in vivo* and *in vitro* experiments to effectively repair biliary damage through suppressing the EGR1/FOS/RAS signaling axis. As a result, a scalable platform for the production of therapeutic OEVs was successfully developed in a 50 mL bioreactor utilizing a matrigel-free methodology, thus offering a bioactive material for liver regeneration.



KEYWORDS: extracellular vesicles, liver ductal organoids, suspension culture, cholangitis, macrophages

Received: March 10, 2025; **Revised:** June 4, 2026
Accepted: June 8, 2026

✉Address correspondence to Zhe Yang, yangzhe_0201730@163.com; Shusen Zheng, shusenzheng@zju.edu.cn; Meijin Guo, guo_mj@ecust.edu.cn; Ali Mohsin, alimohsin@ecust.edu.cn

1 Introduction

Primary sclerosing cholangitis (PSC) is a chronic hepatobiliary disorder characterized by progressive biliary inflammation and hepatic fibrosis, ultimately culminating in extensive hepatocyte necrosis [1, 2]. The development of hepatic fibrosis in PSC is attributed to the release of pro-inflammatory cytokines and

infiltration of immune cells, notably macrophages and T lymphocytes [1, 3]. Liver transplantation is the only available treatment for end-stage liver disease. However, its use is severely constrained by the lack of donor organs, which underscores the pressing demand for novel treatment approaches [4, 5]. Previous studies have demonstrated that biliary epithelial cells (BECs) can serve as bi-potential liver progenitor cells (LPCs) and function as a source of hepatic generation when hepatocyte-mediated liver regeneration is impaired in mice [6–8]. Therefore, therapies based on LPCs/BECs may offer a promising approach for promoting liver regeneration in individuals with PSC.

Recent advancements in organoid culture techniques have established organoids-derived products as promising candidates for regenerative therapies, given their capability to recapitulate multiple cell lineages, such as BECs and LPCs [9, 10]. Previous studies have demonstrated that the transplantation of adult stem cell-derived hepatobiliary organoids can alleviate hepatic fibrosis and facilitate liver regeneration [11, 12]. Nevertheless, despite their significant therapeutic potential, their clinical translation is limited by many challenges, such as their immunogenicity, tumorigenic potentials, and ethical issues [13–16]. To advance organoid-based regenerative therapies for adult liver diseases, researchers need to prioritize the development of therapeutic by-products derived from organoids. Extracellular vesicles (EVs) are nanoscale bilayer lipid vesicles secreted by almost all cell types (including organoids), and are considered a safer and more flexible alternative to cell therapy [17, 18]. EVs can activate cellular processes in the liver regeneration microenvironment via cell-cell communication, such as immune modulation, enhanced proliferation and differentiation [19–21]. Compared to traditional 2D-cultured EVs, organoid-derived extracellular vesicles (OEVs) more accurately resemble the EVs isolated from human bodily fluids. This resemblance is primarily attributed to the unique three-dimensional architecture of organoids and the complex diversity of cell types present within them [22, 23]. Due to their generally low propensity to induce an immune response, OEVs are being investigated as potential "off-the-shelf" treatment options [24–26].

The utilization of OEVs is still in its early stages and faces significant challenges [27–29]. A primary limitation to clinical implementation is the absence of efficient strategies for generating standardized organoids and OEVs at a large scale, while simultaneously reducing manufacturing time and costs [30, 31]. Although engineered approaches have advanced high-quality generation for organoids and OEVs, the complexity of conventional extracellular matrix (ECM) biomimetic strategies introduced additional challenges in the isolation of OEVs [17]. Moreover, the yield of OEVs highly relies on organoids' quantity and their quality is closely correlated with the biological fidelity of the source organoids. A crucial issue for the effective use of engineered EVs in clinical practice is understanding the differentiation pathways of the source organoid [32, 33]. Importantly, another significant barrier to the administration of OEVs is that the precise mechanisms underlying their biological effects are still poorly understood [34, 27]. Existing data derived from experiences with EV utilization have indicated that therapeutic effects may be primarily mediated by specific proteins and nucleic acids enriched within the EVs [35]. Among these, microRNAs (miRNAs) have been involved in regulating the immune microenvironment and inflammation, which are closely related to disease progression [36–38]. Uncertain molecular pathways involved in liver regeneration are likely to limit their widespread clinical use for the foreseeable future. Therefore, we speculate that miRNAs enriched in OEVs could modulate the immune microenvironment and inflammatory responses associated with PSC.

To address these critical challenges, we herein developed a nanobiotechnology platform leveraging liver ductal organoid-derived OEVs for PSC treatment (Fig. 1). Firstly, a matrigel-free suspension culture system was established in a 50 mL bioreactor to generate three distinct cell groups of human liver ductal organoids, which effectively release functional OEVs. Single-cell sequencing analyses revealed that the bioreactor-based suspension culture facilitates the hepatocyte reprogramming into proliferative hepatic progenitor cells, subsequently leading to differentiation into BECs. The 3D OEVs produced by multi-lineage differentiated organoids demonstrated a 25% higher particle-to-protein ratio compared to conventional OEVs isolated from liver ductal organoids grown on multi-well plates (2D OEVs). Secondly, 3D OEVs harvested from human liver ductal organoids were more effective in reducing liver inflammation and fibrosis in 3,3'-diindolylmethane (DDC)-treated mouse models by regulating M1 macrophage polarization. Finally, miRNA profiling analysis of the 3D OEVs identified miR-1299 as a pivotal mediator of their therapeutic effects. The elucidation of the mechanism through which miR-1299, enriched in the 3D OEVs, effectively repairs biliary damage *in vivo* was also conducted. Therefore, a scalable suspension culture for multi-lineage differentiated hepatobiliary organoid-derived EVs was developed in a bioreactor. This advancement provides a promising alternative method for the large-scale preparation of OEVs, offering significant potential for liver disease research and other clinical treatments.

2 Results and discussion

2.1 Generation of high-quality liver ductal organoids cultivated in 3D suspension culture

To facilitate the scalable generation of liver ductal organoids and their OEVs, a matrigel-free suspension culture system was established in a spinner flask bioreactor. Firstly, the generation efficiency and quality of liver ductal organoids cultured under static and dynamic conditions were compared (Fig. 2(a)). As shown in Fig. 2(b), in suspension culture mode, liver ductal organoids were directly generated from adult stem cells without the involvement of matrigel. Over a culture duration of 7 days, the growth rate and size of the organoids in suspension culture more than doubled those observed under static conditions (Figs. 2(c) and 2(d)). The organoids maintained intact typical epithelial organoid morphology in both static and suspension culture modes. Moreover, organoid size in suspension cultures was significantly larger than that observed in static culture conditions. Interestingly, an enhancement in glycolytic activity was evident in the suspension cultures, as evidenced by a 1.3-fold increase in glucose consumption (Fig. 2(e)) and 1.15-fold elevation in lactate production relative to static culture controls (Fig. S1 in the ESM). Furthermore, enhanced lineage specification was also revealed by functional maturation analysis in suspension-cultured organoids. The lineage specification expression of hepatic marker (hepatocyte nuclear factor 4, alpha (HNF4α), albumin (ALB)) and cholangiocytic marker (keratin 19 (KRT19) and KRT7) were significantly elevated compared to those in static controls (Figs. 2(f)–2(h)). These results indicate that the suspension culture system markedly enhances the generation

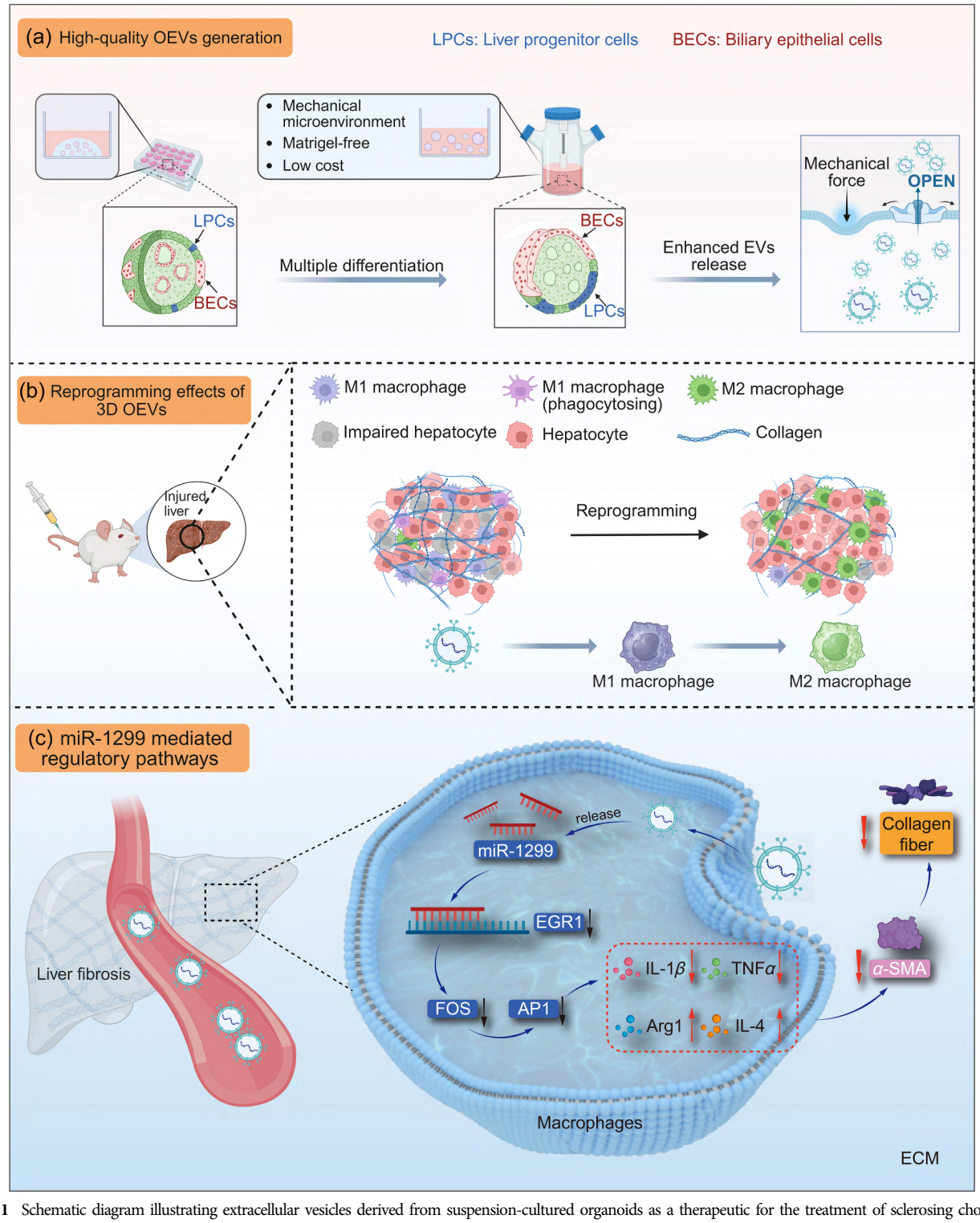


Figure 1 Schematic diagram illustrating extracellular vesicles derived from suspension-cultured organoids as a therapeutic for the treatment of sclerosing cholangitis. (a) Suspension culture promotes multi-lineage differentiation of organoids compared to static culture conditions. (b) Suspension cultured organoid-derived 3D OEV reprogram M1 macrophages toward an M2 phenotype. (c) 3D OEV alleviate hepatic fibrosis and inflammation via miR-1299.

efficiency, growth rate, size, metabolic activity, and functional maturation of liver ductal organoids.

2.2 3D suspension culture promotes the differentiation of liver ductal organoids

To gain a comprehensive understanding of transcriptomic changes induced by modified culture protocols in liver ductal organoids, RNA sequencing was conducted on organoids derived from three distinct liver samples. A total of 2329 significantly differentially expressed genes (DEGs) were identified between the two culture groups (Fig. 3(a)). The heatmap presented in Fig. 3(b) demonstrates the distinct transcriptomic profiles observed in organoids cultured

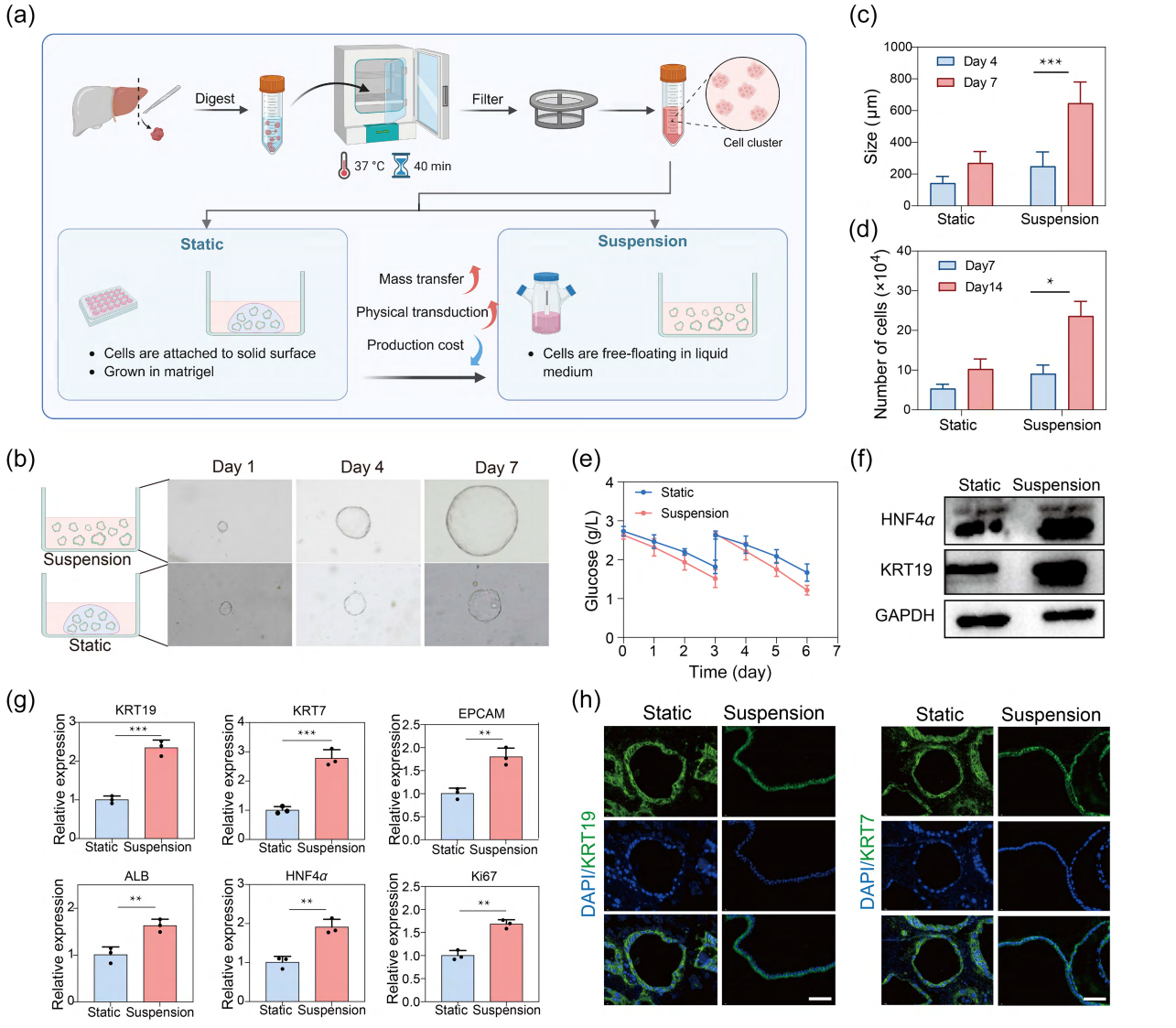


Figure 2 Generation of high-quality liver ductal organoids through matrigel-free suspension culture. (a) Schematic illustration of the induction protocols for liver ductal organoids in static and suspension culture modes. (b) Representative morphology of organoids under different culture modes at days 1, 4, and 7. (c) Size comparison of organoids in different culture modes. (d) Cell number comparison of organoids in different culture modes. (e) Glucose consumption comparison of organoids in different culture modes. Glucose levels in the culture medium were measured. (f) Protein expression levels of hepatobiliary markers in organoids in different culture modes. (g) Relative mRNA expression levels of hepatobiliary markers in organoids in different culture modes. (h) Representative immunofluorescence images of organoids in different culture modes stained with specified antibodies (KRT19 and KRT7). Scale bars: 100 μm. Statistical significance was denoted as $^{*}P < 0.05$, $^{**}P < 0.01$, and $^{***}P < 0.001$.

under suspension cultures compared to those in static conditions. Gene Ontology (GO) and Kyoto Encyclopedia of Genes and Genomes (KEGG) pathway enrichment analyses demonstrated that genes significantly upregulated in suspension-cultured organoids, compared to those in static culture conditions, were predominantly enriched in key biological pathways, including metabolic processes, tissue repair, organic acid transport, and bile secretion (Figs. 3(c) and 3(d), and Figs. S2(a)–S2(d) in the ESM). These findings provide robust evidence that the suspension culture system effectively promotes functional differentiation of liver ductal organoids. Moreover, the biliary properties of the organoids were enhanced by suspension culture. Main markers such as KRT19, KRT7, and other functional biliary markers like gamma-glutamyltransferase 1 (GGT1), aquaporin 1 (AQP1), and polymeric immunoglobulin receptor (PIGR) of liver ductal organoids showed promoted expression patterns in suspension culture mode (Fig. 3(e)). Similarly, the hepatic characteristics of the liver ductal organoids were augmented, with upregulated key regulatory proteins for liver development and function, such as HNF4α and ALB, indicating normal hepatocyte differentiation (Fig. 3(e)). Notably, genes encoding proliferating cell nuclear antigen (PCNA), stathmin 1 (STMN1), and Ki67 related to cell proliferation were highly expressed in the suspension cultured organoids, confirming that suspension culture enhances the growth capability of the organoids.

Further, gene set enrichment analysis (GSEA) and heatmap analysis indicated that the genes exhibiting enhanced expression in suspension culture were predominantly associated with the PI3K-AKT, RAP1, TGF-β, and cell adhesion pathways (Figs. 3(f) and 3(g)). Subsequently, the upregulation of proteins fibronectin (FN1),

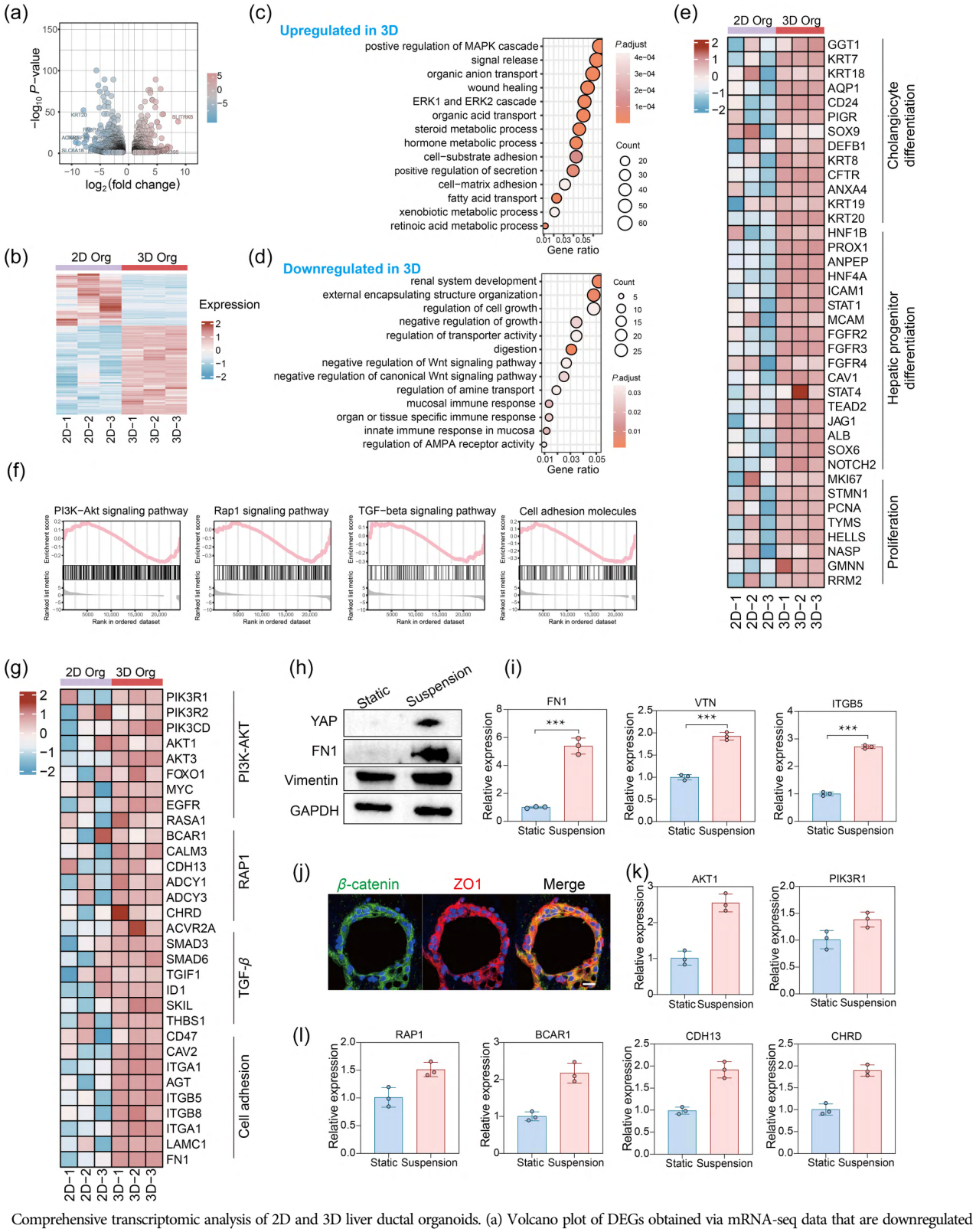


Figure 3 Comprehensive transcriptomic analysis of 2D and 3D liver ductal organoids. (a) Volcano plot of DEGs obtained via mRNA-seq data that are downregulated and upregulated in 3D organoids. (b) A heatmap of DEGs in 3D and 2D cultured liver ductal organoids. GO-term analysis for biological processes of DEGs. (c) upregulated and (d) downregulated in 3D-cultured organoids. (e) A heatmap representing normalized counts of markers related to hepatic markers. (f) GSEA plot showing significant enrichment of Mechanosensitive pathways. (g) A heatmap of DEGs related to the major signaling pathways regulated in 3D-cultured organoids. (h) The protein level of mechanical sensitivity related protein (YAP, FN1, Vimentin) in 2D and 3D cultured organoids. (i) Relative mRNA level of mechanical sensitivity related genes (*VTN*, *FN1*, *ITGB5*) in 2D and 3D cultured organoids. (j) Representative images of immunofluorescence for β-catenin and ZO-1 in liver ductal organoids. Scale bars: 20 μm. Relative mRNA level of (k) PI3K-AKT and (l) RAP1 pathways in 2D and 3D cultured organoids. Statistical significance was denoted as $^{*}P < 0.05$, $^{**}P < 0.01$, and $^{***}P < 0.001$.

Yes-associated protein (YAP), and vitronectin (VTN) were detected in the suspension-cultured organoids (Figs. 3(h) and 3(i)). These findings strongly support the regulatory role of external mechanical-physical signals in the functional differentiation of liver ductal organoids under suspension culture conditions. Immunofluorescence images depicted in Fig. 3(j) demonstrated a phenomenon of partial polarization in the organoids, with a subset exhibiting characteristics of epithelial polarization. This observation prompted us to further investigate the underlying mechanisms, with a particular focus on the role of mechanical forces. An interaction network analysis, derived from the Search Tool for the Retrieval of Interacting Genes (STRING) database, revealed a core module identified by molecular complex detection (MCODE), comprising 20 hub genes and 97 functional associations (Fig. S2(e) in the ESM). This module not only includes mechanical forces-related genes, such as *FN1*, but also cell differentiation-regulated genes with mechanoresponsive characteristics, such as *CXCL1*. Furthermore, relative mRNA levels of genes involved in PI3K-AKT and RAP1 pathways were upregulated in suspension-cultured organoids, which confirmed that suspension culture significantly activated multidimensional molecule pathway (Figs. 3(k) and 3(l)). Further protein analysis demonstrated the upregulation of mechanoresponsive pathway proteins in suspension-cultured organoids, and changes in mechanical force affected the differentiation and maturation of the organoids (Fig. S3 in the ESM). Collectively, these findings indicate that the mechanical microenvironment plays a crucial role in driving the functional maturation of liver ductal organoids through a complex regulatory network.

2.3 Identification of the multi-lineage differentiation of liver ductal organoids for OEVs generation

Single-cell RNA sequencing (scRNA-seq) of suspension-cultured 3D liver ductal organoids was performed. Unsupervised clustering analysis revealed three distinct cellular populations (Chol-0, Chol-1, and Chol-2) (Fig. 4(a)). Notably, it was observed that biliary markers, including *KRT19*, *EPCAM*, *CD24*, and *ANXA4*, were consistently expressed across all clusters (Fig. 4(b)). This indicates that cholangiocyte transcriptional signatures are retained throughout the suspension culture. Unsupervised analysis of DEGs was conducted to characterize the three cellular populations. Chol-0 was marked by a higher expression of *FGFR4*, *CYP3A4*, *HNF4α*, *ABCC3*, which are expressed by hepatic progenitor (Figs. 4(c)–4(e) and Fig. S4 in the ESM). Additionally, genes associated with cell proliferation, including *PCNA*, *TOP2A*, and *Ki67*, were upregulated in the Chol-0. Chol-1 was uniquely defined by stemness cells, representing cholangiocytes in a middle state of differentiation. This middle state of differentiation was evidenced by their high expression of stemness-related genes, including *KLF4*, *RUNX1*, *FOXO3*, and *SOX4* (Figs. 4(c)–4(e) and Fig. S3 in the ESM). Chol-1 also exhibited partial expression of early hepatocyte lineage-defining transcription factors, particularly HNF4α, indicating that these cells are both moderately differentiated and possess stem-like characteristics. The Chol-2 population comprised mature cholangiocytes expressing markers specifically associated with differentiation, such as *NOTCH2*, *KRT7*, *KRT18*, *SOX9*, and *AQP1*, many of which are highly specific to human bile ducts. Violin plots in Fig. 4(f) depict the distribution of three cholangiocyte clusters across organoid types. It is evident that all clusters exhibited a significant expression of biliary markers *EPCAM* and *KRT19*, whereas the hepatic progenitor cluster demonstrated a mature hepatocyte phenotype (*HNF4α*, *ABCC3*). These clusters formed a branching trajectory extending from hepatic progenitors through stem-like intermediates toward cholangiocyte fates, as computed using Monocle2 (Fig. 4(g)). Signature genes expressed in each sub-cluster were identified, with many well-known cholangiocyte markers, including *CD24*, *ANXA4*, and *CD63*, highly enriched in cholangiocytes clusters (Fig. 4(h)). KEGG pathway analysis of the hepatic progenitor subcluster showed enrichment in cell proliferation and metabolic processing pathways, confirming its hepatic progenitor identity (Fig. 4(i)). Moreover, the cholangiocyte sub-cluster exhibited notable enrichment in the PI3K/AKT pathway, consistent with the observed transcriptomic profiles (Fig. S5 in the ESM). Collectively, these findings suggest a gradual hepatic progenitors-to-BEC trans-differentiation via a stemness state in a suspended culture system, thereby elucidating the enhanced hepatobiliary differentiation observed in this dynamic environment as compared to static culture conditions (Fig. 4(j)).

2.4 Characterization of extracellular vesicles derived from liver ductal organoids

The generation of liver ductal organoids has been notably enhanced, leading to the hypothesis that suspension culture not only facilitates organoid formation but also stimulates the secretion of organoids-derived EVs. Based on this, EVs derived from liver ductal organoids were generated under two different culture modes and isolated, defined as 2D organoid derived EVs (2D OEV) and 3D organoid derived EVs (3D OEV) (Fig. 5(a)). Both 3D-OEV and 2D-OEV were found to be nanoscale vesicles with a bilayer membrane (Fig. 5(b)). Subsequently, nanoparticle tracking analysis (NTA) and dynamic light scattering (DLS) were performed on EVs isolated from 2D and 3D culture, ensuring the same cell number and equal volume were used (Figs. 5(c)–5(f)). The sizes of 2D OEV and 3D OEV were approximately 128 and 116 nm. Both types of EVs exhibited good homogeneity, with polydispersity index (PDI) values of 0.3 and 0.2 (Fig. 5(g)). Importantly, particle-to-protein ratio analysis confirmed that 3D OEV preparations exhibited a 1.25-fold increase in particle yield compared to 2D OEV (Fig. 5(i)). Moreover, both 2D OEV and 3D OEV contained the exosome-specific proteins CD9, Alix, and tumor susceptibility 101 (TSG101) (Fig. 5(h)). Notably, compared to 2D OEV, TSG101 expression was significantly upregulated in 3D EVs, which is related to more active EV generation and secretion under the 3D culture mode. The integral endoplasmic reticulum membrane protein Calnexin was not detected in the EVs, indicating high purity of the isolated EVs. Moreover, there were no significant differences observed in zeta potential between the two types of EVs (Fig. 5(j)). In conclusion, 3D OEV derived from suspension-cultured organoids exhibited superior yield and quality compared to 2D OEV.

2.5 OEVs administration alleviates liver fibrosis in PSC model

Besides the yield and quality of 3D OEV, the therapeutic effect of 3D OEV was also tested in a murine model of sclerosing cholangitis according to the protocol (Fig. 6(a)). The mouse recovery was assessed within 30 days. During treatment, the body weight of mice in the DDC diet group was significantly lower than that in the normal group (Fig. 6(b)). Application of 2D OEV and 3D OEV significantly alleviated weight loss. Serum levels of alkaline

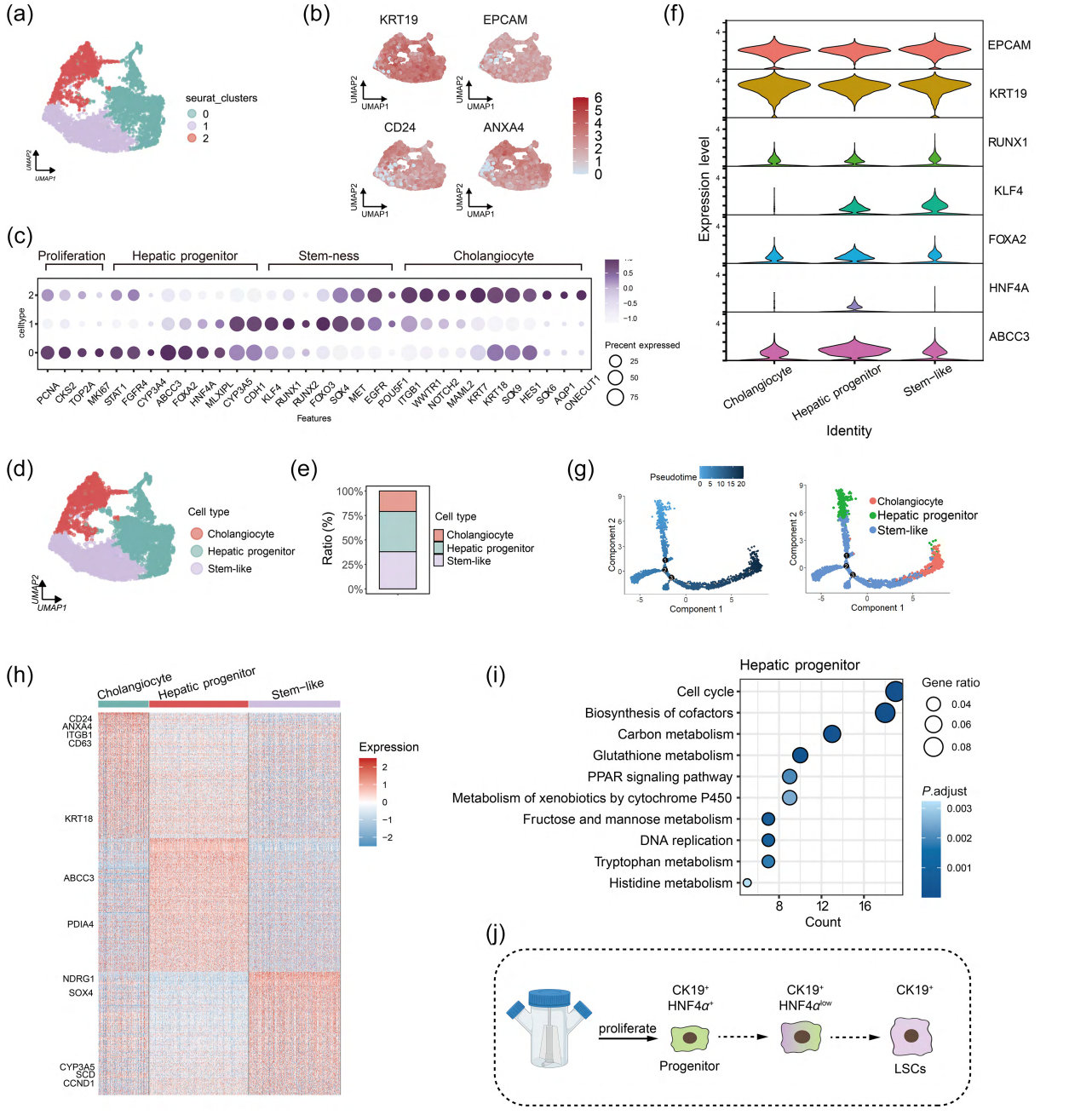


Figure 4 Suspension culture promotes the proliferation of LPCs and differentiation of BECs in liver ductal organoids. (a) Uniform manifold approximation and projection (UMAP) plots of cell clusters from suspension cultured organoids. (b) Feature plots of biliary markers across all clusters from suspension cultured organoids. (c) The dot plot of expression of specific genes to identify different populations of liver ductal organoids. (d) UMAP plots of the distribution of identified populations of cell clusters in suspension cultured organoids. (e) Proportion of identified cell cluster populations in suspension cultured organoids. (f) Violin plots of biliary marker expression in three identified cell clusters from suspension cultured organoids. (g) Pseudotime analysis of three identified cell clusters in suspension cultured organoids. (h) A heatmap of DEGs in three identified cell clusters. (i) KEGG analysis of DEGs in hepatic progenitor cell clusters compared to other clusters. (j) Schematic diagram showing that LPCs proliferated by suspension culture and differentiated into BEC.

phosphatase (ALP), alanine aminotransferase (ALT), and total bilirubin gen. 3 (BILT3) were markedly elevated in the DDC group; however, significantly lower levels of these liver function indicators were found after OEV therapy (Fig. 6(c)). Notably, 3D OEV administration conferred superior anti-fibrotic efficacy compared to 2D OEV, evidenced by significantly downregulated hepatic transcription of fibrosis-associated genes (*TGF-β*, *COL3*, *CTGF*, *TIMP1*, *COL1A1*, and *α*-SMA) (Figs. 6(d)–6(g)). Additionally, biliary injury was also better alleviated by 3D OEV administration with reduced ductal fibrosis and restored biliary architecture (Fig. 6(h)). Relative expression of hepatic bile acid transporter genes (*MDR1*, *MDR2*, *MRP2*, *NTCP*, and *BESP*) increased after treatment, consistent with repaired cholangiocyte damage and improved cholestasis (Fig. 6(i) and Fig. S6 in the ESM). The safety of OEV treatment was also validated; hepatic and renal functions as well as major organs in normal mice remained within normal limits following OEV administration (Fig. S7 in the ESM).

In further analysis, the changes in inflammation symptoms were

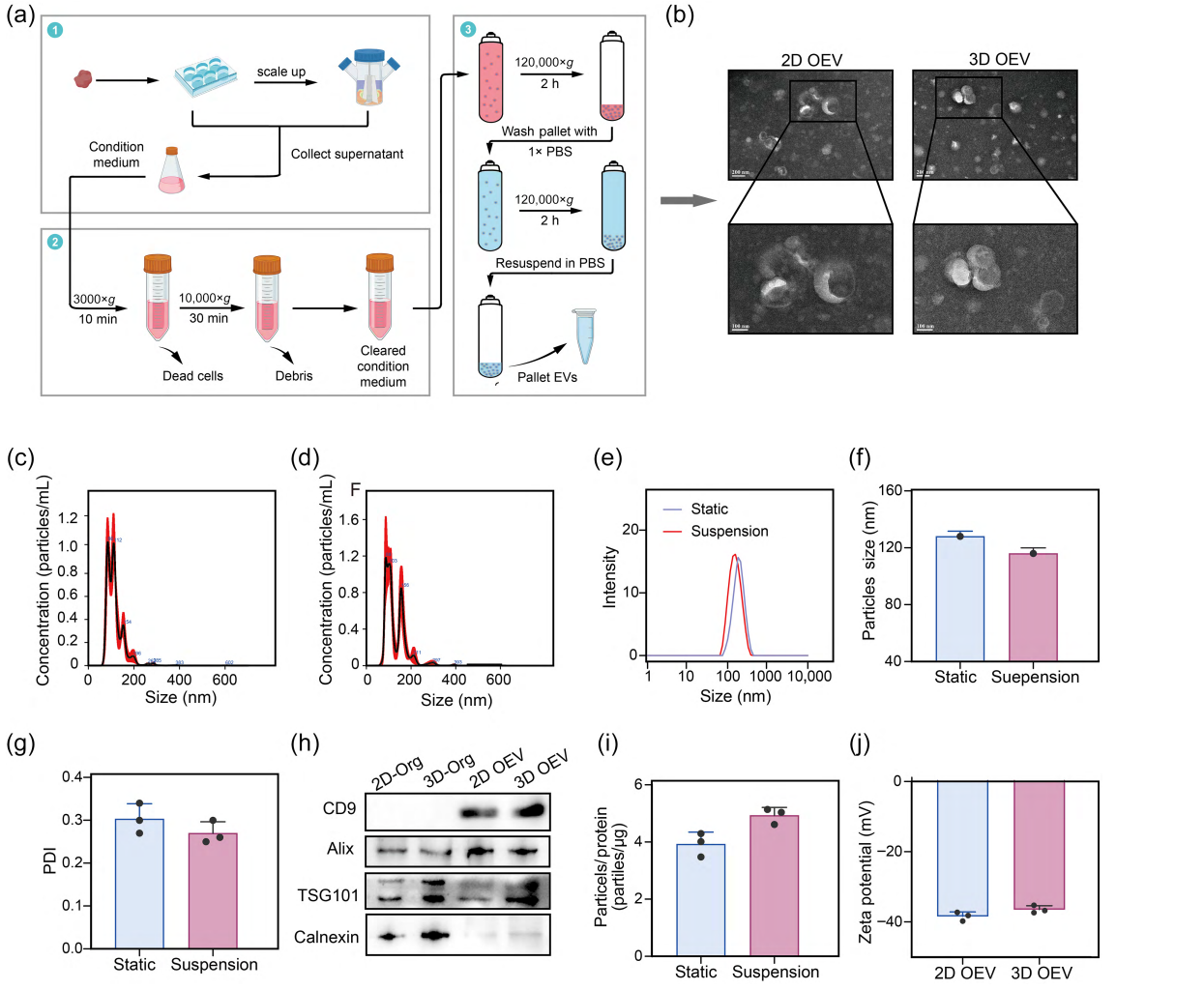


Figure 5 Characterizations of 2D OEV and 3D OEV. (a) Schematic diagram of the EV isolation procedure. (b) TEM images of 2D OEV and 3D OEV. NTA of (c) 2D OEV and (d) 3D OEV. (e) DLS analysis of 2D OEV and 3D OEV. (f) Mean particle size distribution of 2D OEV and 3D OEV. (g) PDI values of 2D OEV and 3D OEV. (h) Protein levels of EV-specific markers (CD9, Alix, TSG101) and negative control Calnexin in 2D OEV and 3D OEV by Western blot. (i) Particles/Protein ratio of 2D OEV and 3D OEV. (j) Zeta potential measurements of 2D OEV and 3D OEV.

examined. Reduced levels of pro-inflammatory mediators (interleukin-1 beta (IL-1β) and tumor necrosis factor-alpha (TNF-α)) and increased anti-inflammatory cytokines (IL-4, arginase 1 (ARG1) and IL-10) were observed after OEV therapy (Figs. 7(a) and 7(b)). Dramatic fluctuation of inflammatory cytokines levels collectively indicated that 3D OEV administration significantly attenuated hepatic inflammation following bile duct injury. Considering that pro-inflammatory cytokines IL-1β and TNF-α are predominantly secreted by macrophages, macrophage dynamics were subsequently investigated during the therapeutic process. The expression of F4/80 was found significantly decreased in the livers of 3D OEV group compared with those in the DDC group and 2D OEV group (Fig. 7(c)). Furthermore, the expression of anti-inflammatory related genes increased as cells developed from M1-type macrophages into M2-type macrophages in the OEV administration group (Figs. 7(d)–7(h)). An obvious increase of $CD11B^{+}/CD206^{+}$ M2-like macrophages was further detected in the 3D OEV group compared to that in the control group (Figs. 7(e) and 7(f)). These findings suggest that 3D OEV therapy may facilitate the polarization of macrophages toward an M2-like phenotype, which may be advantageous for alleviating fibrosis.

2.6 3D OEV secreted by suspension cultured organoids modulate macrophage polarization

To verify the functional interplay between hepatic macrophages and utilized OEVs, an *in vitro* co-culture model of OEVs and M1-type macrophages was established (Fig. 8(a)). As a comparison, a higher accumulation of 3D OEV was observed in M1 macrophages compared to 2D OEV (Fig. 8(b)). Lower expression of inflammatory markers was also detected in 3D OEV, potentially attributed to enhanced differentiation and functional augmentation promoted by suspension culture (Fig. 8(c)). Macrophages treated with lipopolysaccharide (LPS) and interferon-gamma (IFN-γ) were identified as M1 macrophages due to their high CD86 expression. Notably, further analysis indicated that the expression of M1 markers (CD86, IL-1β, TNF-α, and inducible nitric oxide synthase (iNOS)) in M1 macrophages treated with OEV was significantly lower than that in the phosphate buffered solution (PBS) group (Figs. 8(d)–8(f)). In contrast, the protein level of the M2 marker ARG1 was markedly upregulated after 3D OEV treatment. The polarization toward the M2 phenotype was promoted by 3D OEV in both M1 and M2 macrophages using two cell lines (RAW264.7

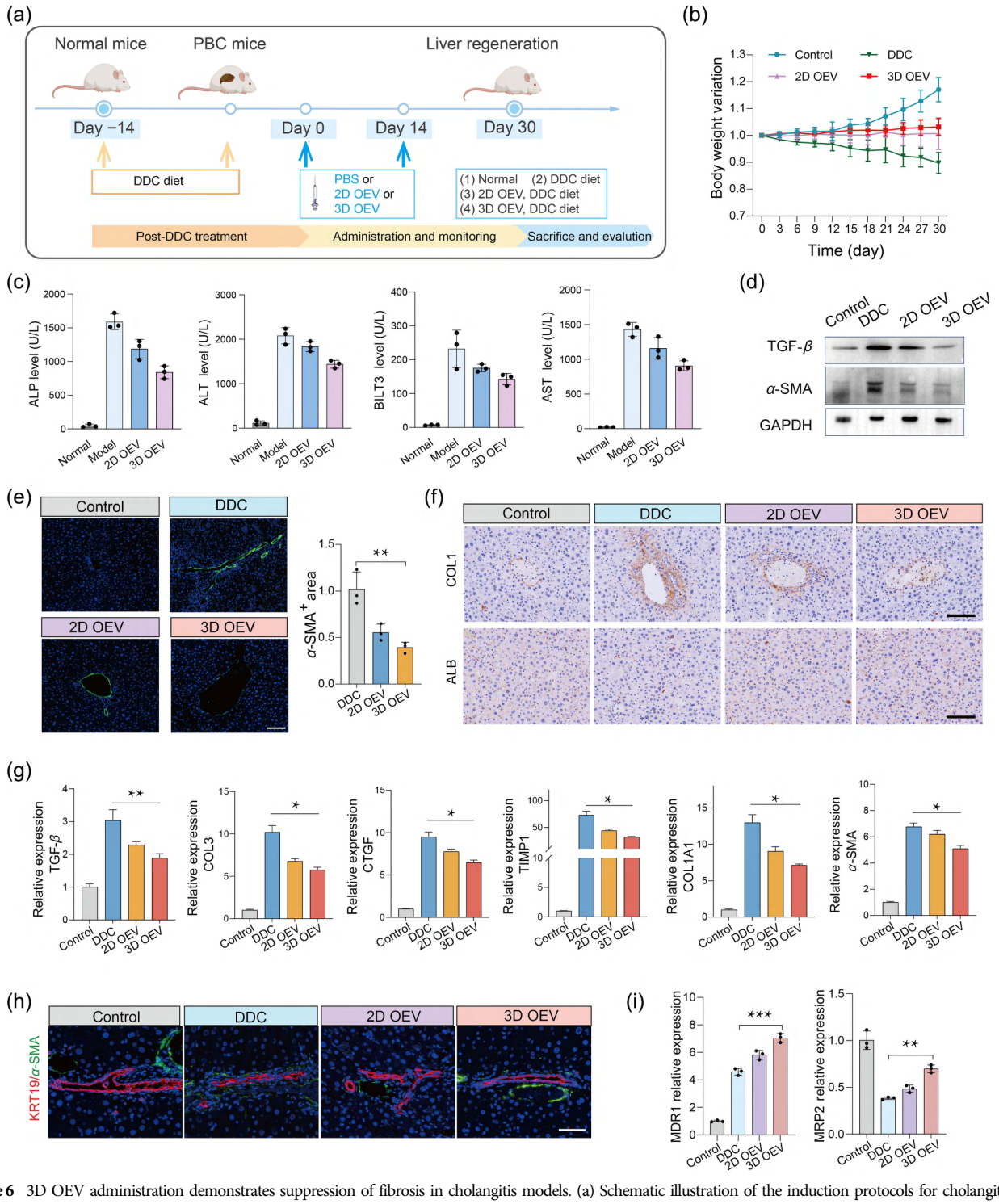


Figure 6 3D OEV administration demonstrates suppression of fibrosis in cholangitis models. (a) Schematic illustration of the induction protocols for cholangitis and OEVs administration. (b) Changes in mouse body weight during the treatment period (n = 5). (c) Liver function tests in mouse blood across experimental groups (n = 3). (d) Protein levels of fibrosis-associated markers in different groups. (e) Representative immunohistochemistry images of α-SMA staining and quantification of the α-SMA staining area. Scale bar: 100 μm. (f) Immunohistochemical staining of COL1 and ALB in the injured liver of mice treated with 2D OEV and 3D OEV. Scale bars: 100 μm. (g) Relative mRNA expression levels of fibrosis-related genes in the injured liver of mice treated with 2D OEV and 3D OEV. (h) Representative immunohistochemical (IHC) staining of α-SMA and Krt19 in bile ducts. Scale bar: 100 μm. (i) Relative mRNA expression levels of cholestasis-related genes in different groups. Statistical significance was denoted as $^{*}P < 0.05$, $^{**}P < 0.01$, and $^{***}P < 0.001$.

and THP1) (Fig. 8(f), and Figs. S8–S10 in the ESM). Flow cytometry analysis revealed that a large amount of CD206 (23.5% and 37.3%) was expressed on M1 macrophages incubated with 2D OEV and 3D OEV, while the expression of CD86 was decreased to 60.7% and 37.6% (Figs. 8(g) and 8(h)). Overall, a stronger polarization toward M2 phenotype was observed in M1 macrophages after being treated with 3D OEV compared with 2D OEV.

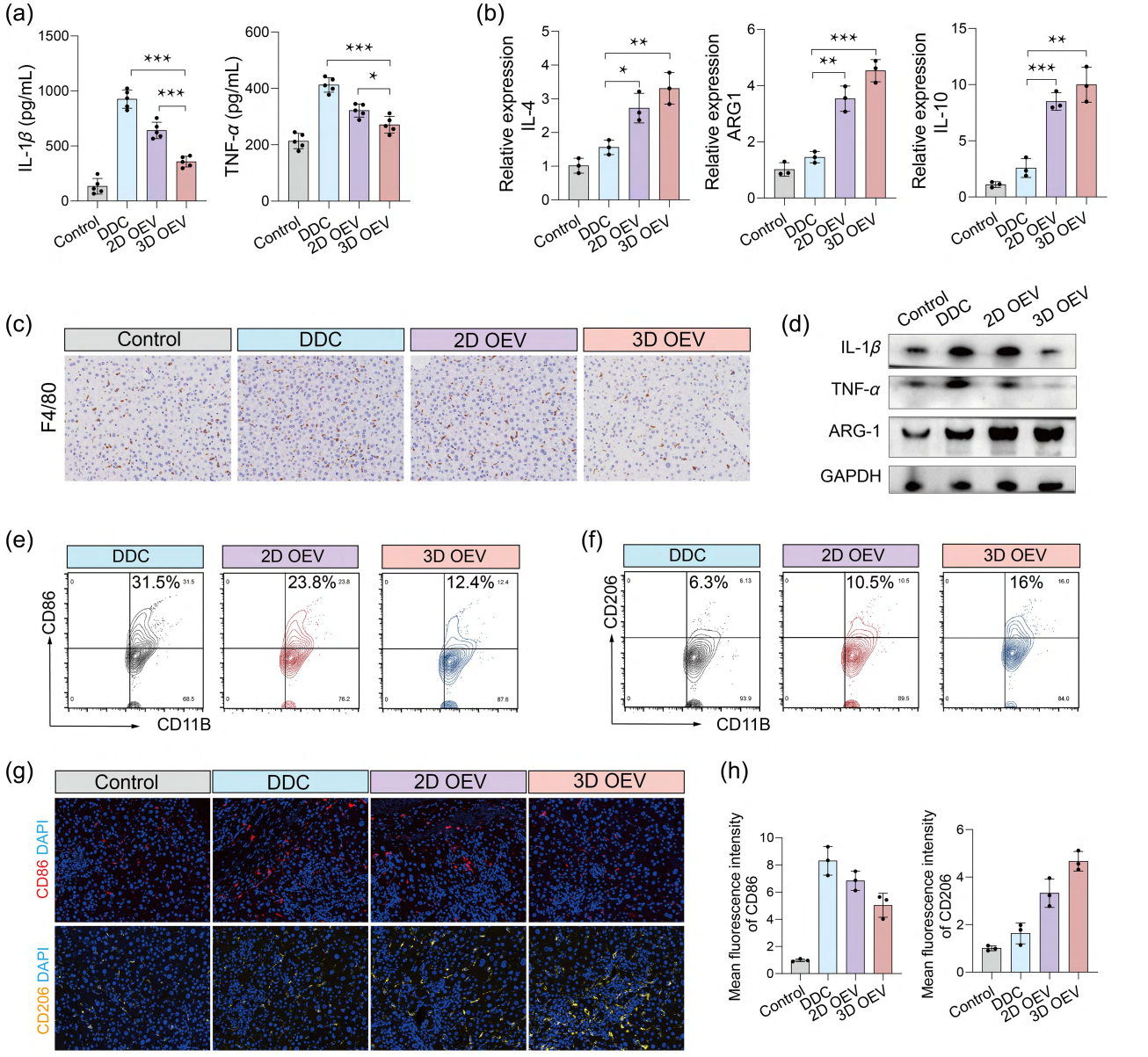


Figure 7 3D OEV administration reprogrammed M1 macrophages toward the M2 phenotype in cholangitis models. (a) Measurement of IL-1β and TNF-α in serum (n = 5). (b) Relative expression of genes of anti-inflammatory M2-type macrophages in liver tissue (IL-4, ARG-1, IL-10) (n = 3). (c) Immunohistochemical staining of F4/80 in the injured liver of mice treated with 2D OEV and 3D OEV. (d) Protein levels of pro-inflammatory (IL-1β, TNF-α) and anti-inflammatory related proteins in liver tissues. Flow cytometric analysis of (e) M1-type and (f) M2-type macrophage markers in liver after treatments with 2D OEV and 3D OEV. (g) Immunofluorescence staining images of M1 marker (CD86) and M2 marker (CD206) in liver tissues. (h) Quantitative analysis of $CD86^+$ and $CD206^+$ stained areas. Statistical significance was denoted as $^*P < 0.05$, $^{**}P < 0.01$, and $^{***}P < 0.001$.

Next, further experiments were performed to check whether 3D OEV-induced macrophage polarization could regulate hepatocyte function, and M1 macrophages post-treated with 3D OEV were co-cultured with AML12 hepatocytes (Fig. 8(i)). The results showed that the expression of hepatocyte markers (ALB, Ki67, HNF4α, and transferrin (TRF)) were upregulated in AML12 cells activated by treated macrophages (Fig. 8(j)). Moreover, it was noted that macrophages treated with 3D OEV could significantly promote hepatocyte proliferation (Figs. 8(k) and 8(l)). Consistent with this, the protein expression level of the proliferation marker Ki67 was also markedly increased (Figs. 8(m) and 8(n)). These findings indicated that 3D OEV therapy can indeed influence hepatocyte function through macrophage mediation.

2.7 3D OEV therapy reduces inflammation and promotes macrophage polarization by regulating FOS expression

After confirming that 3D OEV derived from suspended liver ductal organoids directly mediated the M1-to-M2 macrophage polarization, RNA-sequencing was performed to explore transcriptional differences in M1 macrophages after different treatments. Significantly down-regulation of 1842 and 213 genes were found in macrophages treated with 3D OEV (3D OM) compared to M1 macrophages and 2D OEV treated macrophages (2D OM), with 129 common genes downregulated across both comparisons (Figs. 9(a)–9(c)). Hierarchical-clustering analysis comparing the global gene expression profiles of M1 macrophages, 2D OM and 3D OM confirmed a strong suppression of specific

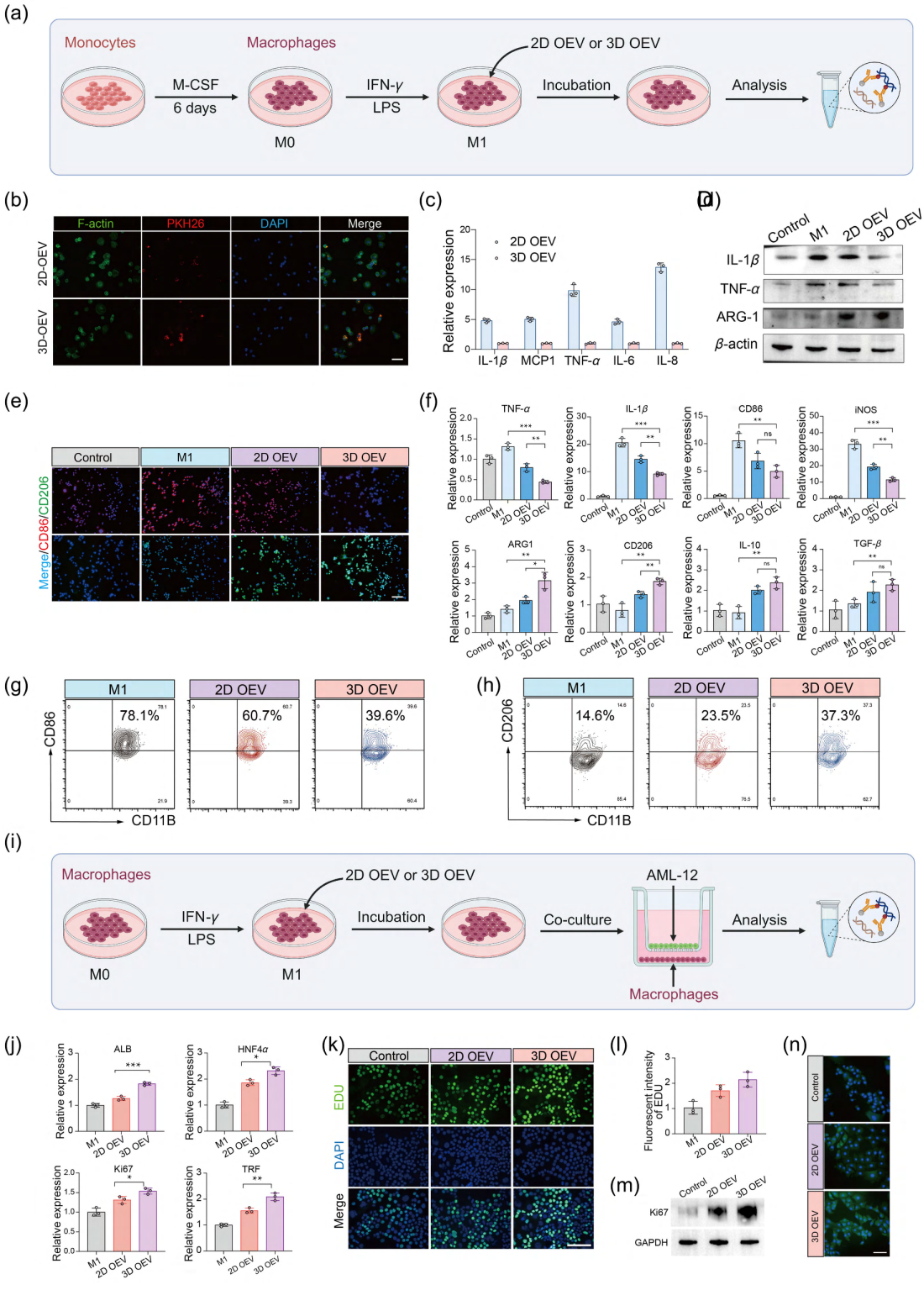


Figure 8 Detection of the *in vitro* reprogramming effects of 3D OEV. (a) Schematic diagram of the model for the reprogramming efficiency of 3D OEV *in vitro*. (b) Qualitative comparison of 2D OEV and 3D OEV uptake by macrophages. Scale bar: 50 μm. (c) Relative mRNA expression of pro-inflammatory genes in 2D OEV and 3D OEV. (d) Protein levels of M1 macrophage markers (IL-1*β*, TNF-*α*) and M2 macrophage markers (ARG1) in RAW264.7 macrophages after incubation with 2D OEV and 3D OEV. (e) Immunofluorescence images of CD86 (red) and CD206 (green) expression in M1 macrophages following treatment with 2D OEV and 3D OEV, with 4',6-diamidino-2-phenylindole (DAPI) staining of nuclei. Scale bar: 200 μm. (f) Relative mRNA expression of M1 markers and M2 markers in M1 macrophages following different treatments. Flow cytometric analysis of (g) M1-type and (h) M2-type markers in M1 macrophages after treatments with 2D OEV and 3D OEV. (i) Schematic diagram of proliferative evaluation model mediated by macrophage reprogramming *in vitro*. (j) Relative mRNA levels of ALB, HNF4*α*, Ki67 and TRF in AML-12 cells co-cultured with post-treated M1 macrophages. (k) EDU staining images of AML-12 cells co-cultured with post-treated M1 macrophages. (l) Relative fluorescent intensity of EDU staining images in panel (k). (m) Protein levels and (n) immunofluorescence images of Ki67 in AML-12 cells co-cultured with post-treated M1 macrophages. Statistical significance was denoted as $^{*}P < 0.05$, $^{**}P < 0.01$, and $^{***}P < 0.001$.

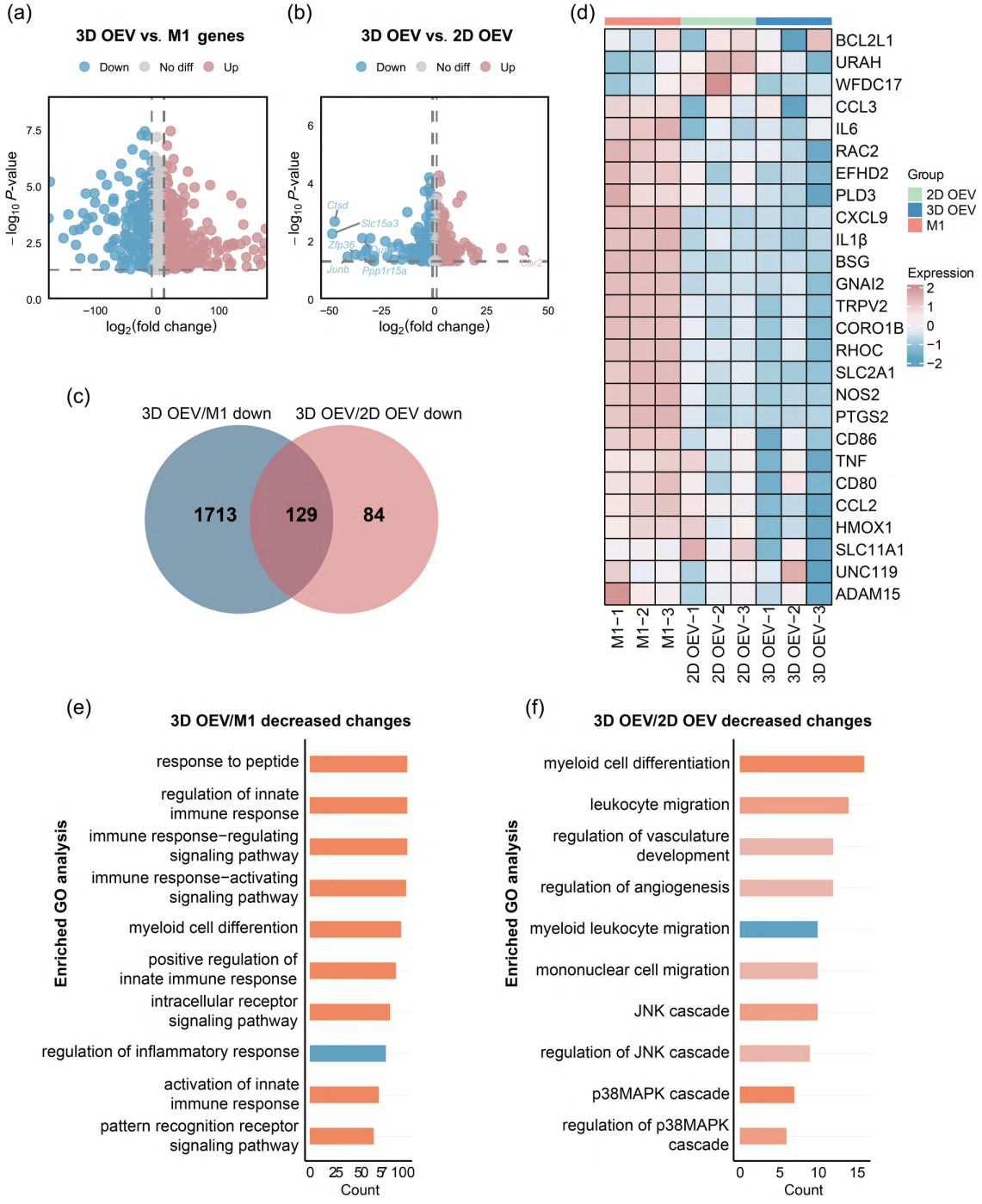


Figure 9 3D OEV promote macrophage polarization by regulating FOS expression. Volcano plot of DEGs obtained via mRNA-seq data that are downregulated and upregulated in 3D OEV treated-M1 macrophages compared to (a) M1-polarized control and (b) 2D OEV-treated M1 macrophages. (c) Venn diagram of commonly down-regulated DEGs in 3D OEV-treated macrophages compared to M1-polarized controls and 2D OEV-treated groups. (d) A heatmap of inflammation related genes in three groups (M1 macrophages, 2D OEV-treated M1 macrophages and 3D OEV-treated M1 macrophages). GO-term analysis for biological processes of DEGs in 3D OEV-treated macrophages compared to (e) M1-polarized controls and (f) 2D OEV-treated group.

genes (CD86 and TNF-α) in OEV-treated macrophages. Of note, 3D OEV exhibited superior reprogramming capacity than 2D OEV in facilitating macrophage phenotype switching. Furthermore, inflammatory factors (such as IL-6, IL-1β, CD86, CD80) and chemokines (such as C-C motif chemokine ligand 2 (CCL2), CCL3, C-X-C motif chemokine ligand 9 (CXCL9)) were highly decreased after treatments with 3D OEV (Fig. 9(d), and Figs. S11(a) and S11(b) in the ESM). Given the central regulatory role of M1 macrophages in hepatic inflammation, OEV therapy may suppress cytokine/chemokine production in M1 macrophages, therefore attenuating cholangitis-associated liver fibrosis.

GO enrichment analysis of the 1842 and 213 DEGs identified that biological processes, including immune system activation and myeloid cell differentiation, were substantially downregulated in 3D OM. These findings indicate that 3D OEV treatment alters the immune phenotype of M1 macrophages (Figs. 9(e) and 9(f)).

Protein interaction network analysis of 129 commonly downregulated DEGs revealed a core module containing 6 hub genes and 12 functional associated genes, all of which functionally drive inflammatory progression (Figs. S11(c) and S11(d) in the ESM). To evaluate the core genes of M1 macrophages targeted by 3D OEV, the CytoHubba plugin with three algorithms in Cytoscape was used. FOS, as a key AP-1 transcription factor component, was identified as a central gene (Fig. S11(e) in the ESM). Previous studies have demonstrated that FOS is a crucial transcription factor in driving the progression of inflammation. Consistent with this finding, the relative FOS gene expression in M1 macrophages was found to be effectively suppressed after 3D OEV treatment (Fig. S11(f) in the ESM). Protein co-expression network analysis also revealed that 3D OEV treatment induced downregulation of key genes functionally enriched in immunomodulatory pathways, including chemokine binding (Fig. S11(g) in the ESM). These data indicated that the inhibition of FOS by 3D OEV promotes M1-to-M2 macrophage activation.

2.8 Enriched miR-1299 in 3D OEV represses the inflammation mediator FOS

To explain the differential effects of 2D OEV and 3D OEV on macrophage polarization observed in *in vitro* and *in vivo* experiments, RNA-seq was carried out to analyze differential miRNA expression profiling between the two groups. Forty miRNAs were significantly upregulated and 7 miRNAs downregulated in 3D OEV compared with 2D OEV (Figs. 10(a) and 10(b)). To identify transcription factors that regulate FOS in M1 macrophages treated with 3D OEV, potential transcription factors targeting FOS were predicted using different databases (Fig. 10(c)). Four candidate transcription factors (Zic family member 3 (ZIC3), MAF bZIP transcription factor B (MAFB), early growth response 1 (EGR1), forkhead box K1 (FOXK1)) were tested, and EGR1 was most significantly suppressed in macrophages treated with 3D OEV than that in the 2D OEV group (Fig. 10(d)). After that, 408 potential miRNAs targeting EGR1 were predicted by the Targetscan database. Seven overlapping miRNAs were found in the overlap between the predicted miRNAs and upregulated miRNAs in 3D OEV (Fig. 10(e)). Among them, miR-1299, miR-143-3p, and miR-199a-3p were found to be expressed higher in 3D OEV than in 2D OEV (Fig. 10(f)). Further experiments demonstrated that miR-1299 significantly inhibited FOS transcription while miR-143-3p and miR-199a-3p had no effect (Fig. 10(g)). Suppressed protein levels of EGR1 and FOS confirmed that miR-1299 is the key miRNA mediating immunomodulatory effects of 3D OEV (Fig. 10(h)). Bioinformatics analysis of miR-1299 target genes revealed that GO biological processes were primarily enriched in immune response-activating signaling pathway and Wnt signaling pathway-related genes (Fig. 10(i)). In terms of KEGG pathways, inflammation and fibrosis related pathways, such as Ras pathways, mTOR pathways, FoxO pathways, and TGF-β pathways, were highlighted (Fig. 10(j)). Notably, cellular senescence signaling pathways were found to be targeted by miR-1299, which indicates potential links between these pathways and 3D OEV-promoted tissue regeneration. Based on these results, it was hypothesized that miR-1299 enriched in 3D-OEV might regulate macrophage polarization via the EGR1/FOS/RAS axis.

In order to explore this hypothesis, transfection of miR-1299 mimics in 293T cells reduced luciferase activity of wild-type EGR1 but not mutant EGR1, confirming EGR1 as a direct target of miR-1299 (Figs. 10(k) and 10(l)). Additionally, Ras pathway-related gene expression was significantly reduced in 3D OEV-treated macrophages compared with 2D OEV-treated controls (Fig. 10(m)). These results collectively demonstrate that 3D OEV drive M2 macrophage polarization through miR-1299-mediated suppression of EGR1/FOS/RAS axis activation in macrophages.

2.9 MiR-1299 enriched in 3D OEV promotes M2 macrophage polarization

To confirm that miR-1299 is the miRNA in 3D-OEV that exerts a major effect on promoting M2 polarization, macrophages were treated with 3D-OEV *in vitro* with or without the addition of a miR-1299 inhibitor (Fig. 11(a)). The experimental data consistently showed that the protein expression of M1 markers, including TNF-α, IL-1β and CD86, was significantly decreased in macrophages treated with 3D-OEV. In contrast, there was an observed increase in M2 markers (ARG1, IL-10, CD206) in these cells (Figs. 11(b)–11(e)). Furthermore, a significant increase in $CD11B^{+}$/CD86 macrophages from 54.6% to 70.8% in M1 macrophages following administration of the miR-1299 inhibitor was detected, with the $CD11B^{+}$/CD206 decreasing from 22.6% to 15.8% (Figs. 11(f) and 11(g)).

Subsequently, co-culture of AML12 with macrophages was conducted, which was post-treated with 3D OEV or 3D OEV + miR-1299 inhibitor (Fig. 11(h)). 5-ethynyl-2'-deoxyuridine (EDU) staining data showed that macrophages treated with the miR-1299 inhibitor had a negative effect on the proliferation of AML12 (Fig. 11(i)). Metabolites of medium from AML12 cultures were further detected, which indicated the suppression of glycolysis induced by the miR-1299 inhibitor (Figs. 11(j) and 11(k)). Furthermore, the expression of hepatocyte markers (ALB, Ki67, HNF4α, and TRF) was downregulated in AML12 after incubation with miR-1299 inhibitor-treated macrophages (Fig. 11(l)). Additionally, after inhibition of miR-1299, the proliferation of co-cultured AML12 cells was downregulated, as evidenced by corresponding Ki67 expression (Fig. 11(m)). All these results above indicate that miR-1299-mediated M2 macrophage polarization promotes hepatocyte growth and functional enhancement.

2.10 MiR-1299 attenuated hepatic inflammation and fibrosis, promoting M2 macrophage polarization *in vivo*

In vitro analysis revealed that miR-1299 is enriched in 3D OEV and repairs liver injury through the promotion of macrophage polarization. To test this hypothesis *in vivo*, DDC-treated mice were treated with 3D OEV with or without a miR-1299 inhibitor (Fig. 12(a)). The results showed that 3D OEV administration improves the weight loss in DDC treated mice, whereas that of the miR-1299 inhibitor group was significantly suppressed (Fig. 12(b)). Moreover, the beneficial effects of 3D OEV on hepatic function recovery were essentially annihilated by concurrent addition of the miR-1299 inhibitor (Fig. 12(c)). An increase of α-SMA and TGF-β expression in mice treated with 3D OEV + miR-1299 inhibitor was revealed, which proved that liver fibrosis was aggravated in the presence of the miR-1299 inhibitor (Fig. 12(d)). Consistent with these findings, histological analysis revealed exacerbated liver fibrosis upon miR-1299 inhibition, which was characterized by increased collagen deposition and ECM production (Fig. 12(e)). This pathological progression was further confirmed by

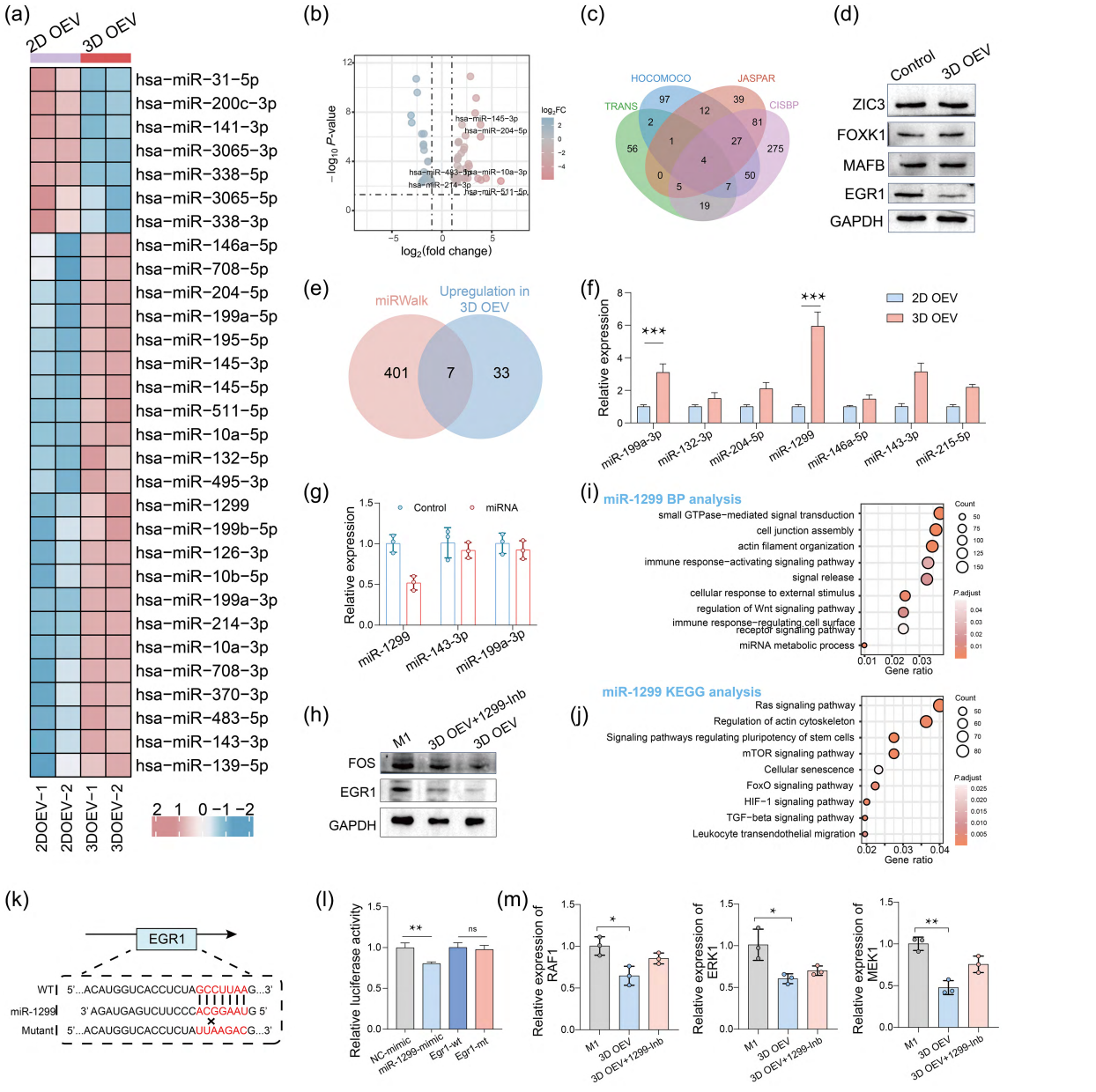


Figure 10 Enriched miR-1299 in 3D OEV represses the inflammation mediator FOS. (a) Heatmap showing differentially expressed miRNAs by miRNA-seq analysis of 2D OEV and 3D OEV. (b) Volcano plot of differentially expressed miRNAs that are downregulated and upregulated in 3D OEV compared to those in 2D OEV. (c) Venn diagram of transcription factors targeting FOS predicted by different databases (TRANS, HOCOMOCO, JASPER and CISBP). (d) Protein levels of potential transcription factors in M1 macrophages after 3D OEV treatment. (e) Venn diagram of predicted miRNAs targeting EGR1 overlapping with miRNAs enriched in 3D OEV. (f) Relative miRNA expression levels in 2D OEV versus 3D OEV. (g) FOS mRNA expression in M1 macrophages treated with miR-1299, miR-143-3p, or miR-199a-3p mimics. (h) Protein levels of FOS and EGR1 in M1 macrophages treated with 3D OEV or 3D OEV + miR-1299 inhibitor. (i) GO biological process analysis of miR-1299 target genes. (j) KEGG pathway enrichment of miR-1299 target genes. (k) Predicted binding site of miR-1299 within the 3'UTR of EGR1. (l) Dual-luciferase reporter assay for verifying interaction between miR-1299 and EGR1. (m) Relative expression of Ras pathway genes (*RAF1*, *EEK1*, *MEK1*) in M1 macrophages treated with 3D OEV or 3D OEV + miR-1299 inhibitor. Statistical significance was denoted as $^{*}P < 0.05$, $^{**}P < 0.01$, and $^{***}P < 0.001$.

upregulated expression of liver fibrogenic genes (Fig. 12(f), and Figs. S12 and S13 in the ESM). Moreover, the miR-1299 inhibitor significantly reduced ALB expression, indicating impaired hepatic function (Fig. 12(g)). Furthermore, the presence of the miR-1299 inhibitor led to the upregulation of EGR1, FOS and RAS pathway genes (Fig. 12(h)). These *in vivo* findings collectively demonstrate that miR-1299, enriched in 3D OEV, plays a crucial role in modulating the EGR1/FOS pathway.

Previous research has indicated that M1-type macrophages are repolarized into anti-inflammatory M2 macrophages during treatment, which contributes to the amelioration of fibrosis. The phenotypic characteristics of macrophages, with or without the miR-1299 inhibitor, were subsequently analyzed. The administration of the miR-1299 inhibitor increased macrophage infiltration and impaired the ability of 3D OEV to reprogram M1 macrophages toward the M2 phenotype (Figs. 12(i)–12(l)). Analysis of macrophage-associated proteins confirmed elevated expression of M1 (TNF-α, IL-1β, and iNOS) markers and reduced M2 marker (ARG1, IL-4, and IL-10) levels following miR-1299 inhibition. The proportion of CD86/CD11B M1 macrophages increased from

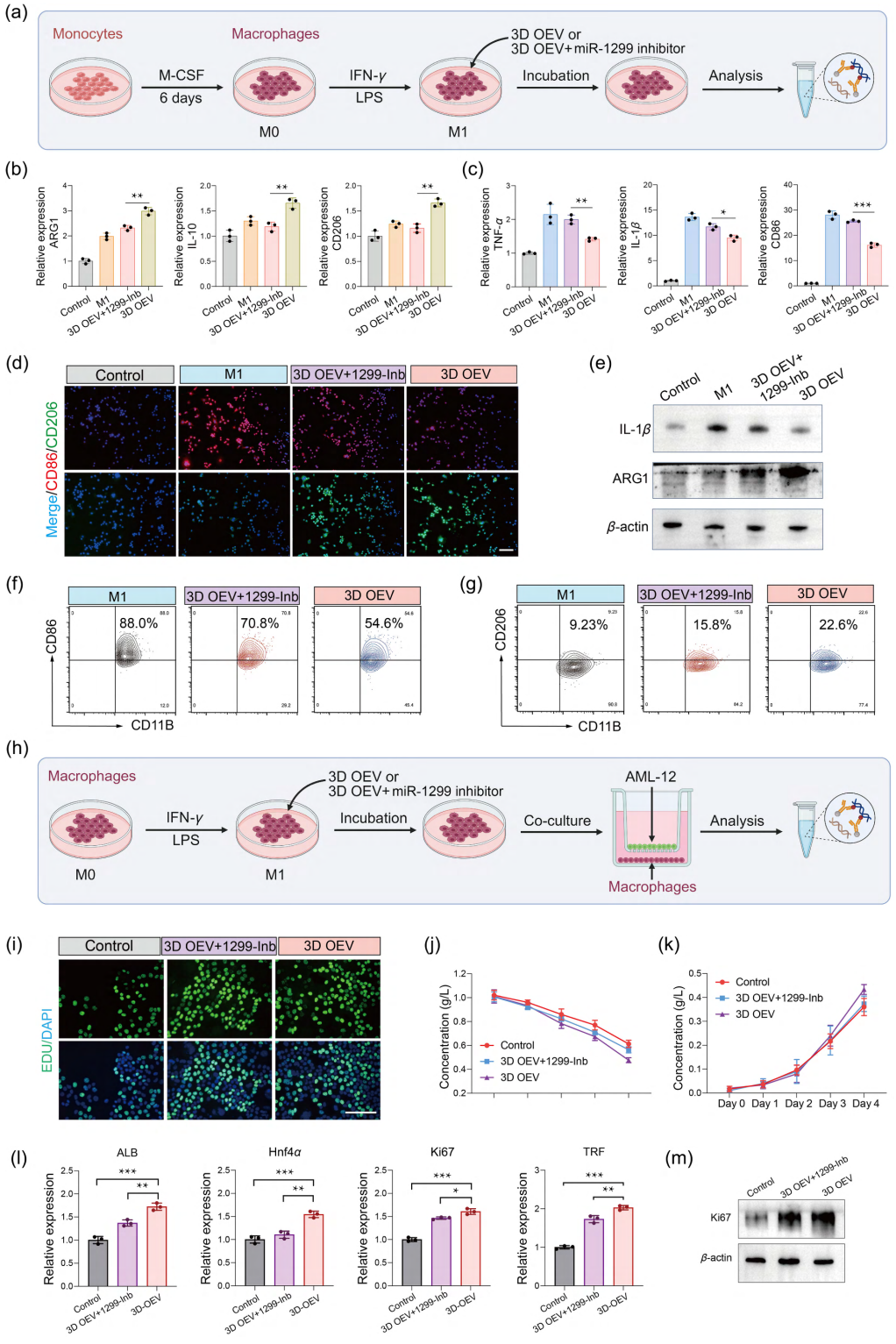


Figure 11 Enriched miR-1299 in 3D OEV promotes M2 macrophage polarization. (a) Schematic diagram of the model for the reprogramming efficiency of enriched miR-1299 in 3D OEV. Relative mRNA expression of (b) M2 markers (ARG1, IL-10, CD206) and (c) M1 markers (TNF-α, IL-1β, CD86) in M1 macrophages after different treatments. (d) Immunofluorescence images of CD86 (red) and CD206 (green) expression in M1 macrophages following treatment with 3D OEV and 3D OEV + miR-1299 inhibitor, with DAPI staining of nuclei. (e) Protein levels of M1 macrophage markers (IL-1β) and M2 macrophage markers (ARG1) in M1 macrophages after treatments with 3D OEV and 3D OEV + miR-1299 inhibitor. Flow cytometric analysis of (f) CD86 and (g) CD206 markers in M1 macrophages after treatments with 3D OEV and 3D OEV + miR-1299 inhibitor. (h) Schematic diagram of proliferative evaluation model mediated by macrophage reprogramming *in vitro*. M1 macrophages were post-treated with 3D OEV or 3D OEV + miR-1299 inhibitor. (i) EDU staining images of AML-12 cells co-cultured with post-treated M1 macrophages. (j) Glucose consumption and (k) lactic acid generation of AML-12 cells co-cultured with post-treated M1 macrophages. (l) Relative mRNA levels of ALB, Hnf4α, Ki67, and TRF in AML-12 cells co-cultured with post-treated M1 macrophages. (m) Protein levels of Ki67 in AML-12 cells co-cultured with post-treated M1 macrophages. Statistical significance was denoted as $^{*}P < 0.05$, $^{**}P < 0.01$, and $^{***}P < 0.001$.

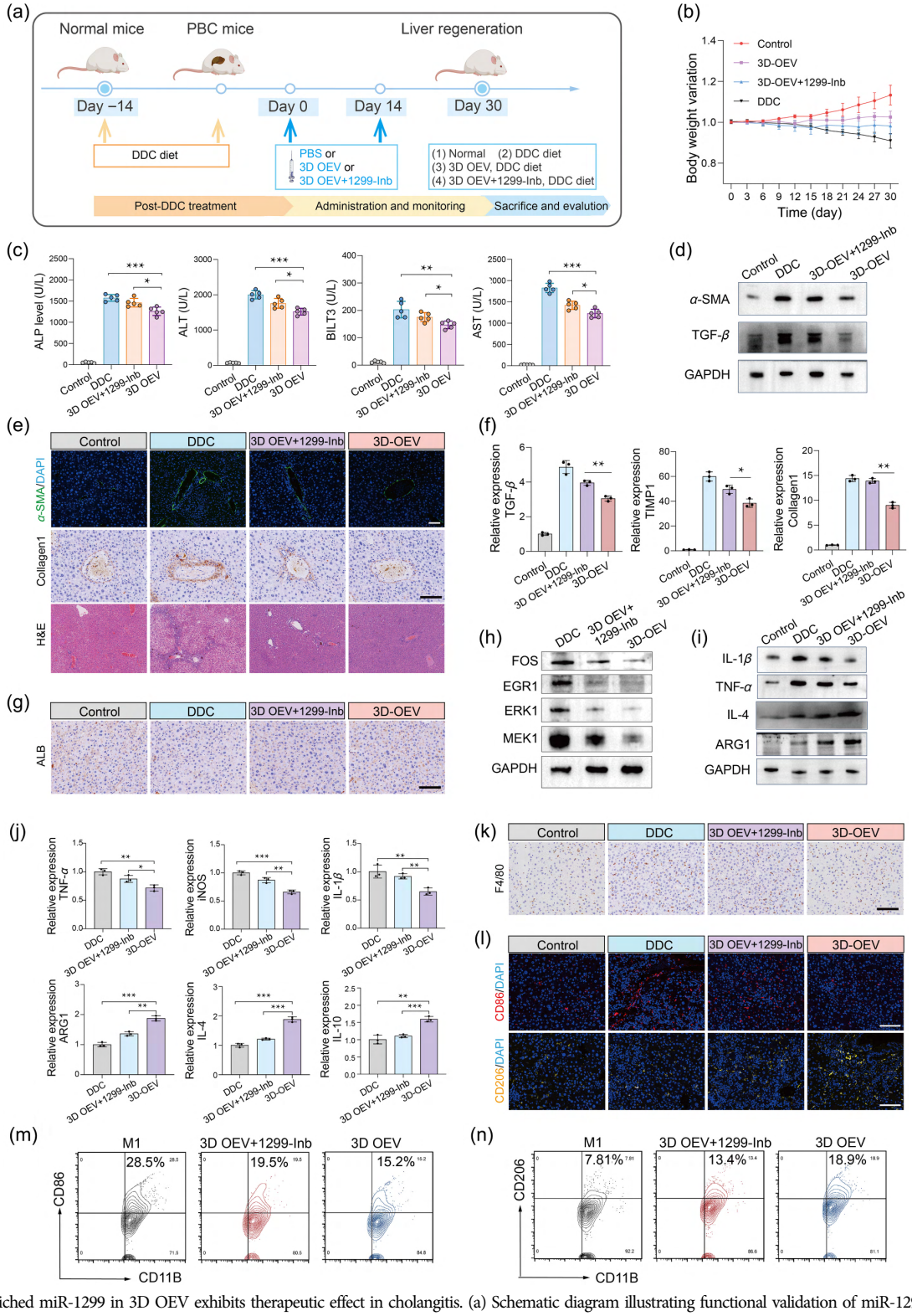


Figure 12 Enriched miR-1299 in 3D OEV exhibits therapeutic effect in cholangitis. (a) Schematic diagram illustrating functional validation of miR-1299 delivered via OEV administration. (b) Changes in mouse body weight during the treatment period (n = 5). (c) Measurement of ALP, ALT, BILT3, and AST in serum (n = 5). (d) Protein levels of fibrosis-associated proteins (TGF-β and α-SMA) in different groups. (e) Histological assessment of hepatic fibrosis severity. α-SMA and COL1 were immunostained respectively. Scale bars: 100 μm. (f) Relative mRNA expression levels of cholestasis-related genes in different groups. (g) Immunohistochemical staining of ALB in the injured liver of mice in different groups. Scale bar: 100 μm. (h) Protein levels of FOS, EGR1, ERK1 and MEK1 in the injured liver of mice treated with 3D OEV or 3D OEV + miR-1299 inhibitor. (i) Protein levels of pro-inflammatory (IL-1β, TNF-α) and anti-inflammatory (ARG1, IL-4) related proteins in livers. (j) Relative mRNA expression of M1 markers (IL-1β, TNF-α, and iNOS) and M2 markers (ARG1, IL-4, and IL-10) in livers. (k) Immunohistochemical staining of F4/80 in the injured liver of mice in different groups. Scale bar: 100 μm. (l) Immunofluorescence staining images of M1 marker (CD86) and M2 marker (CD206) in livers. Flow cytometric analysis of (m) M1-type and (n) M2-type markers in liver after treatments with 3D OEV and 3D OEV + miR-1299 inhibitor. Statistical significance was denoted as $^{*}P < 0.05$, $^{**}P < 0.01$, and $^{***}P < 0.001$.

15.2% to 19.5% in the absence of miR-1299, whereas the proportion of CD206/CD11B M2 macrophages decreased from 18.9% to 13.4% (Figs. 12(m) and 12(n)). In conclusion, these findings indicate that miR-1299, enriched in 3D OEV, effectively modulates the EGR1/FOS pathway and facilitates the reprogramming of macrophages, thereby providing significant therapeutic potential for the treatment of liver diseases.

3 Discussion

Here, we attempted to develop a stably scalable liver ductal organoid from human primary hepatocytes to mimic *in vivo* hepatobiliary physiology and subsequently generate functional EVs. In the matrigel-free suspension culture system, robust proliferation of bipotent hepatic progenitor cells was observed, concomitant with the promotion of differentiation into hepatic stem cells. Notably, the study demonstrated the effective function of EVs released from these matrigel-free cultured organoids. Compared with 2D OEV, miR-1299 enriched 3D OEV were more effective in alleviating hepatic fibrosis and biliary injury, as well as promoting M2 macrophage polarization in DDC-treated mice. These results reveal a novel mechanism through which utilized organoid-derived EVs modulate the recipient immune microenvironment, highlighting their potential utility in the treatment of primary biliary injury. Nevertheless, future studies are needed to optimize the process control of organoid scalable culture and the dosing of extracellular vesicle administration.

(1) Matrigel-free suspension culture in bioreactors enables scalable generation of functional OEVs from liver ductal organoids

Nowadays, organoids derived from adult stem cells exhibit significant potential for medical applications, particularly in transplantation therapy, owing to the close reproducibility of the cellular diversity of their source tissues [9, 11]. To date, studies have reported that administration of both organoids and OEVs can induce regeneration of damaged tissues [17, 39]. However, the advantages of organoid-based therapies in the field of regenerative medicine are constrained by their culturing efficiency, as ensuring a substantial cell yield is crucial to meet the demands of organoid-based therapy. Organoid engineering strategies that promote the culture, growth, proliferation, differentiation, and maturation of organoids have been reported [40–42]. Generally, OEVs generation employs two distinct culture modalities: static culture and suspension culture. Static culture involves embedding cells within an ECM, which supports cellular development into organoids within culture wells [43]. In contrast, suspension culture refers to the cultivation of organoids directly in liquid medium without adhesion [44–46]. In previous studies, OEVs have been successfully generated in static culture and applied in tissue regenerative medicine [22, 47]. Static cultured OEVs still face several challenges: (1) The extracellular matrix frequently contains animal-derived components, which may compromise the reliability of organoid-based therapy; (2) full standardization is lacking in conventional static culture protocols, contributing to increased reagent and labor costs for scaling up cell production; (3) OEV isolation is influenced by the proteins and other components in matrigel. Moreover, matrigel digestion with enzymes may compromise OEV integrity. These factors pose additional challenges for OEV isolation. To overcome the drawbacks of static OEVs culture, suspension culture offers a novel approach for large-scale OEVs production, which potentially bypasses limitations of extracellular matrix and boosts OEVs quality. Herein, we developed a matrigel-free culture system in flask bioreactors to expand organoid cultivation as well as enhance production efficiency and functionality: (1) High-quality organoids exhibited significantly higher growth rates, with an average diameter 2.6-fold larger than static cultured organoids (Fig. 2); (2) suspension culture enhanced the expression of hepatobiliary markers (HNF4α and KRT19) (Fig. 3); (3) 3D OEV generation was more efficient and functional, with a 1.25-fold increase in particle-to-protein ratio compared to 2D OEV (Fig. 5). Consequently, the matrigel-free culture system reported here enables the robust generation of functional OEV.

The quality of OEVs was profoundly influenced by the cellular composition and properties of donor-derived organoids. Cell culture in bioreactors effectively promotes the proliferation, multilineage differentiation, and survival of progenitor cells, consequently improving both the quality and yield of OEVs. In contrast, inadequate oxygenation and the use of matrigel pose significant obstacles to high-quality OEV production in static culture systems. Although previous studies have reported bioreactor-facilitated organoid generation, the differentiation dynamics of donor organoids under suspension conditions remain elusive [48, 49]. In this study, single-cell transcriptomic analysis was employed to characterize liver ductal organoids cultured in suspension culture. We have now identified a subset of hepatic progenitors in suspension cultured organoids, which are characterized by a hybrid EPCAM/HNF4α gene expression signature. This subset represents bipotent transitional hepatic progenitors, capable of transdifferentiating into hepatocytes during liver regeneration following injury [7]. Furthermore, a distinct KRT19^{+}/CD63 cholangiocyte-like hepatic stem cell subset, which contributed to restoring hepatic parenchymal mass following injury, was identified at the differentiation endpoint [50]. Thus, liver ductal organoids help repair wounds after injury driven by the dynamic differentiation of these two cell subsets. Comparative transcriptomic analysis between static and suspension cultured organoids revealed significant upregulation of hepatocyte-specific markers (*Alb*, *Hnf4α*, *Cyp3A4*), biliary markers (*Krt19*, *Krt7*), and proliferation-associated genes (*PCNA*, *TOP2A*) in suspension culture conditions (Fig. 3(e)). Notably, mechanical force-related genes, including *YAP*, *FN1*, and *Vimentin*, were highly enriched in dynamically cultured organoids (Figs. 3(h) and 3(i)). Furthermore, GSEA analysis revealed that most of the top-upregulated GO terms in suspension cultured organoids were associated with regeneration functions, such as bile secretion, wound healing, and PI3K signaling. These findings indicate that the proliferation and differentiation of hepatic progenitor cells into biliary epithelial-like hepatic stem cells was promoted in suspension culture, thereby enhancing lineage plasticity and tissue regeneration. Further study is needed to elucidate the mechanisms underlying cell fate determination and differentiation plasticity during suspension culture.

(2) miR-1299-enriched OEVs derived from suspension cultured liver ductal organoids attenuate liver fibrosis via macrophage reprogramming

As suspension cultured liver ductal organoids highly expressed the gene signatures for cell proliferation, differentiation, and wound healing, we further evaluated the pro-regenerative capacity of OEVs in DDC-treated mice. While studies on EVs released by suspension-cultured organoids for cell-free therapy are limited, we demonstrate the therapeutic efficacy of EVs derived from suspension-cultured organoids for the first time. Firstly, OEVs showed higher yield,

homogeneity, and purity in suspension culture than in static condition. Moreover, polarization of M1 to M2 macrophages was observed in the inflammatory condition, by which biliary injury and hepatic fibrosis were mitigated in DDC-treated mice. Given this, we investigated the molecular cargo within EVs responsible for modulating the hepatic microenvironment. miR-1299 was proven to play a critical role as an anti-inflammatory effector mediating the beneficial effects of 3D OEV in DDC-treated mice. Notably, inhibition of miR-1299 greatly abrogated the therapeutic impact of 3D OEVs in this model. Transcriptomic analysis further elucidated that suppression of FOS constitutes the primary pathway through which miR-1299 facilitates M1 macrophage repolarization. The proportion of M2 macrophages was increased in the livers of DDC-treated mice with the downregulation of FOS, consequently reducing ductular reaction and hepatic fibrosis.

Building upon the remarkable therapeutic efficacy demonstrated in this study, future strategies utilizing suspension cultured organoids-derived EVs from human primary hepatocytes for autologous or allogeneic therapy show great potential as a promising immunotherapy. When considering clinical translation, subsequent investigations should prioritize the following key aspects: (1) Further investigations are required to elucidate the plasticity of cell-fate decisions during suspension culture. Synergistic interplay between mechanical cues and the metabolic microenvironment must be imperatively dissected, with particular emphasis on the dynamic expression kinetics of master transcription factors such as HNF4*α*. This aims to enhance the functional stability of secreted EVs. (2) Engineering biotechnologies should be developed to enhance the targeting specificity of EVs, including parental modification, chemical surface modification, membrane fusion, and electroporation. These engineering strategies must balance precision with safety, thereby augmenting tissue selectivity and minimizing systemic exposure. (3) The development of bioreactor platforms tailored for organoids is urgently demanded. Key parameters of advanced bioreactors include real-time monitoring of organoid diameter, EV secretion kinetics, and critical metabolite gradients. Urgent establishment of GMP-compliant standards for such devices, which encompass closed-loop tubing and in-line sterile sampling, is essential. (4) In the future, further in-depth investigation is needed to explore other potentially synergistic miRNAs and to perform comparative analyses of hepatobiliary organoids and their OEVs derived from different sources of liver tissues (such as different age groups of donors) in order to reveal broader regulatory networks. The use of hepatobiliary organoids derived from iPSCs could establish a more stable and scalable sample acquisition system, thereby supporting larger-scale omics analyses and functional validation. These follow-up studies will further improve the molecular mechanism map of OEVs and promote their clinical translation. Overall, concerted interdisciplinary efforts should be prioritized to accelerate the bench-to-bedside translation of OEV therapies.

4 Conclusions

A novel matrix-free culture strategy was established for generating high-quality 3D OEV with therapeutic potential for PSC. 3D OEV produced under suspension culture exhibited improved uniformity, yield, and therapeutic efficacy compared to those from conventional static 2D cultures. These enhancements resulted from promoted multidirectional differentiation and proliferation of liver ductal organoids in suspension, mechanistically supported by mechanoresponsive signaling pathways as revealed through single-cell and transcriptomic sequencing. Compared to 2D OEV, 3D OEV more effectively alleviated inflammation and fibrosis in a cholangitis mouse model and promoted polarization of M1 macrophages toward the M2 phenotype. Integrated transcriptome and miRNA sequencing identified miR-1299 as a key mediator facilitating M2 macrophage polarization via targeting the EGR1/FOS signaling axis. Both *in vivo* and *in vitro* evidence support 3D OEV therapy as an effective cell-free therapeutic strategy for biliary regeneration.

5 Experimental

5.1 Preparation and culture of human liver organoids

Liver tissues were collected during liver procedures at Shulan (Hangzhou) Hospital, Hangzhou, China. The study received ethical approval from the institutional ethics committees of the Shulan (Hangzhou) Hospital (KY2025078). Firstly, liver specimens were mechanically minced with scissors into about 1 mm^3 cubes, and the tissue fragments were washed with PBS for 3 times to remove impurities. Then, the tissue fragments were enzymatically digested with DMEM/F12 containing 0.1 mg/mL DNase I and 0.5 mg/mL collagenase type III for 30 min at 37 °C. The cell clusters trapped on the 100 μm filters were collected and suspended in DMEM/F12 and centrifuged at 300×*g* for 5 min. The precipitated cell clusters were resuspended in human culture medium and placed in one well of non-treated 6-well plates with 3 mL culture medium (HepatiCult™ Organoid Kit, Stemcell). The 6-well plates were transferred into the orbital shaker in a 37 °C incubator as soon as possible. The shaker was set at 90 r/min. After every two days, the 6-well plate can be angled to allow the organoids to settle, after which the medium can be carefully aspirated and replaced with fresh medium.

5.2 Detection of the growth of organoids

To detect the growth of organoids, microscopes were used to take photographs of the organoids on the first, third and seventh day, respectively. The sizes of organoids under different culture modes were measured, and then the average sizes were calculated. To detect the viability of organoids, suspension cultured liver ductal organoids were collected and washed twice with PBS. Then the organoids were incubated with DMEM/F12 containing 10 mg/mL collagenase type III for 30 min at 37 °C. The cell suspension from the digested organoids was centrifuged and collected for use. An automatic cell fluorescence analyzer was used to determine the viability of organoids (CountStar Mira FL, Shanghai Ruiyu Biotech Co., Ltd., China).

5.3 OEVs preparation and isolation

Liver ductal organoids were cultured in static and suspension conditions. The culture was collected and centrifuged (300×*g*, 10 min) to eliminate dead cells, then the clear supernatant was subjected to centrifugation again (10,000*g*, 30 min) to get rid of cell debris. After that, the supernatant was filtered through a 0.22 μm sterile filter and ultracentrifuged twice (120,000*g*, 2 h) to collect EVs. The extracellular vesicles were resuspended in PBS and stored at −80 °C for later use.

5.4 Characterization of 2D OEV and 3D OEV

Transmission electron microscopy (TEM, JEM-2100, Japan) was

used to observe the morphological and dimensional properties of 2D OEV and 3D OEV. NTA (Particle Metrix, Germany) was used to measure the concentration of OEVs. Total protein was extracted from organoids in two culture conditions and the characteristic markers (CD9, Alix, TSG101 and Calnexin) were validated by Western blot. The average size, size dispersion, and surface charge of the nanomaterials including 2D OEV and 3D OEV were assessed by means of a Zeta Potential and Particle Sizer (Malvern ZS90, UK) to assess their dispersibility and stability.

5.5 Detection of the reprogramming effects of OEV *in vitro*

M0 macrophages (RAW264.7) were seeded in 6-well plates. To induce M1 polarization, M0 macrophages were treated with 20 ng/mL recombinant murine IFN-γ (Peprotech, USA) for 48 h, followed by 50 ng/mL LPS (Beyotime, China) for an additional 4 h. To verify the reprogramming effect of OEVs, M1 macrophages were treated with either 2D OEV or 3D OEV. To investigate the role of miR-1299 enriched in 3D OEV, M1 macrophages were treated with 3D OEV alone or 3D OEV combined with a miR-1299 inhibitor. After 24 h, the macrophages were harvested for further analysis.

5.6 Co-culture of AML-12 with reprogrammed macrophages

M1 type macrophages were prepared according to previous protocols. To verify the reprogramming effect of OEVs, the M1-type macrophages were treated with 2D OEV or 3D OEV. To verify the important effect of miR-1299 enriched in 3D OEV, the M1-type macrophages were treated with 3D OEV + miR-1299 inhibitor or 3D OEV alone. After 24-h incubation, the supernatant was replaced with fresh culture medium. A trans-well chamber was used to co-culture post-treated macrophages with AML-12 cells. After 48 h, proliferation of AML-12 cells was detected by EDU staining. Additionally, the expression levels of hepatocyte-related biomarkers (ALB, HNF4α, Ki67, and TRF) were assessed by qPCR.

5.7 Establishment of mouse model

Six-week-old C57BL/6 male mice were purchased from Shanghai Model Organisms (Shanghai, China) and housed under controlled 12-h light and dark cycles. All procedures of the animal experiments have been approved by the institutional animal care and use committee of Shanghai Jiaotong University (Ethical Approval Number: A2025357). From day −14 to 0, mice were fed a 0.1% DDC diet. DDC can promote the accumulation of protoporphyrin, damage the biliary epithelium, and cause liver injury.

5.8 Administration of OEVs or miRNA inhibitor in mouse model

To verify the therapeutic effect of 2D OEV or 3D OEV, mice were divided into four groups: (1) the normal control group, (2) PBS group, (3) 2D OEV treatment group, and (4) 3D OEV treatment group, with five mice in each group. For OEV treatments, mice were intravenously administered with 2D OEV and 3D OEV (50 μg/mouse, once a week). To verify the important effect of miR-1299 enriched in 3D OEV, mice were divided into four groups: (1) the normal control group, (2) PBS group, (3) 3D OEV + miR-1299 inhibitor group, and (4) 3D OEV treatment group, with five mice in each group. For the miRNA experiments, 3D OEV (50 μg/mouse, once a week) and antagomir-1299 (RiboBio Co., Ltd., 20 nM/0.1 mL/mouse, once a week) were intravenously injected into each mouse. The experiments started from day 0. The health status of the mice was monitored daily, and body weight was recorded every two days. On day 30, all mice were euthanized.

5.9 Single cell RNA-Seq

Organoids derived from suspension culture were collected and subjected to single cell RNA sequencing by Applied Protein Technology (Shanghai, China). Firstly, single-cell suspensions were prepared in PBS at a final concentration of 1×10^6 cells/mL. The calculated volume of cell suspension required to generate 10,000 GEMs (Gel Bead-in-Emulsions) per sample was loaded onto the Chromium Controller (10× Genomics). Libraries were constructed using the Chromium v3 Single Cell 3' Library & Gel Bead Kit (10× Genomics) according to manufacturer specifications. Final library quantification and quality control were carried out with the Agilent DNA 1000 Kit (Agilent Technologies, USA), followed by sequencing on the Illumina NovaSeq 6000 platform (Illumina, USA). The Seurat package (v3.1.5 R) was used to perform downstream analysis.

5.10 Statistical analysis

Data are presented as mean ± standard error of the mean (SEM) from at least three independent experiments. Statistical analysis was performed using GraphPad Prism. Significance levels were defined as $^*P < 0.05$, $^{**}P < 0.01$, and $^{***}P < 0.001$. Comparisons among multiple groups were conducted using one-way ANOVA.

Electronic Supplementary Material: Supplementary material (primer sequences, bioinformatics analysis data, and cellular experimental data) is available in the online version of this article at https://doi.org/10.26599/NR.2026.94908921.

Data availability

Additional data related to this paper may be requested from the corresponding author upon request.

Acknowledgements

This study was supported by grants from the National Natural Science Foundation of China (No. 82470690), the Key Research and Development Project of Zhejiang Province (No. 2024C03149), the Fundamental Research Funds for the Central Universities (No. 2025ZFJH03), Hainan Province Science and Technology Special Fund (No. ZDYF2025LCLH012), the Key R&D Program of China (No. 2023YFC2306800). We thank BioRender.com for expert assistance in the drawing of the cartoon-style pictures.

Declaration of competing interest

All the contributing authors report no conflicts of interest in this work.

Author contribution statement

S. Y. G.: Conceptualization, investigation, methodology, validation, visualization, writing – original draft. Y. L.: Conceptualization, investigation, methodology, visualization. X. Y. L., Y. W. H., Q. B.

Y.: Formal analysis, funding acquisition, investigation, resources. Z. Y.: Conceptualization, funding acquisition, investigation, resources, visualization. S. S. Z. and M. J. G.: Conceptualization, data curation, methodology, project administration, resources, writing – review & editing. A. M.: Investigation, methodology, project administration, funding acquisition, resources, writing – review & editing.

Informed consent

The clinical data, perioperative specimens, and related images presented in this case report were used under institutional ethical approval (Ethics code: KY2025078). All data were de-identified to protect patient privacy.

Ethics statement

Liver tissues were collected during liver procedures at Shulan (Hangzhou) Hospital, Hangzhou, China. The study received ethical approval from the institutional ethics committees of the Shulan (Hangzhou) Hospital (Ethics code: KY2025078).

All procedures of the animal experiments have been approved by the institutional animal care and use committee of Shanghai Jiaotong University (Ethical Approval Number: A2025357). All animal procedures were performed in accordance with the National Institute of Health Guide for the care and use of laboratory animals.

Use of AI statement

This work utilized Grammarly's Generative AI just to improve the English language of the text. The authors fully reviewed and accurately edited the content as needed and take full responsibility for the published article's content.

References

[1] Guillot, A.; Winkler, M.; Silva Afonso, M.; Aggarwal, A.; Lopez, D.; Berger, H.; Kohlhepp, M. S.; Liu, H. Y.; Özdirik, B.; Eschrich, J. et al. Mapping the hepatic immune landscape identifies monocytic macrophages as key drivers of steatohepatitis and cholangiopathy progression. *Hepatology* **2023**, *78*, 150–166.

[2] Trivedi, P. J.; Hirschfield, G. M.; Adams, D. H.; Vierling, J. M. Immunopathogenesis of primary biliary cholangitis, primary sclerosing cholangitis and autoimmune hepatitis: Themes and concepts. *Gastroenterology* **2024**, *166*, 995–1019.

[3] Andrews, T. S.; Nakib, D.; Perciani, C. T.; Ma, X. Z.; Liu, L.; Winter, E.; Camat, D.; Chung, S. W.; Lumanto, P.; Manuel, J. et al. Single-cell, single-nucleus, and spatial transcriptomics characterization of the immunological landscape in the healthy and PSC human liver. *J. Hepatol.* **2024**, *80*, 730–743.

[4] Lucey, M. R.; Furuya, K. N.; Foley, D. P. Liver transplantation. *N. Engl. J. Med.* **2023**, *389*, 1888–1900.

[5] Qiao, Y. B.; Li, J. H.; Bian, S. C.; Zhan, C. Y.; Luo, J.; Jiang, L.; Li, H. Y.; Wu, H.; Zhang, C.; Zheng, S. S. et al. Application of biocompatible custom ceria nanoparticles in improving the quality of liver grafts for transplantation. *Nano Res.* **2023**, *16*, 5176–5188.

[6] Gadd, V. L.; Aleksieva, N.; Forbes, S. J. Epithelial plasticity during liver injury and regeneration. *Cell Stem Cell* **2020**, *27*, 557–573.

[7] Pu, W. J.; Zhu, H.; Zhang, M. J.; Pikiolek, M.; Ercan, C.; Li, J.; Huang, X. Z.; Han, X. M.; Zhang, Z. Q.; Lv, Z. et al. Bipotent transitional liver progenitor cells contribute to liver regeneration. *Nat. Genet.* **2023**, *55*, 651–664.

[8] Johnson, R. L. Hippo signaling and epithelial cell plasticity in mammalian liver development, homeostasis, injury and disease. *Sci. China Life Sci.* **2019**, *62*, 1609–1616.

[9] Tang, X. Y.; Wu, S. S.; Wang, D.; Chu, C.; Hong, Y.; Tao, M. D.; Hu, H.; Xu, M.; Guo, X.; Liu, Y. Human organoids in basic research and clinical applications. *Signal Transduct. Target. Ther.* **2022**, *7*, 168.

[10] Ma, W. J.; Xu, Y. X.; Gu, Z. F.; Li, D. Advanced strategies in organoids for metabolic monitoring and metabolic disease modeling. *Nano Res.* **2026**, *19*, 94907988.

[11] Sampaziotis, F.; Muraro, D.; Tysoe, O. C.; Sawiak, S.; Beach, T. E.; Godfrey, E. M.; Upponi, S. S.; Brevini, T.; Wesley, B. T.; Garcia-Bernardo, J. et al. Cholangiocyte organoids can repair bile ducts after transplantation in the human liver. *Science* **2021**, *371*, 839–846.

[12] Gong, S. Y.; He, K. X.; Liu, Y.; Luo, X. Y.; Ashraf, K.; He, J. Z.; Li, W. F.; Yang, L. H.; Rehman, T. U.; Shen, M. W. et al. Scalable matrigel-free suspension culture for generating high-quality human liver ductal organoids. *Cell Prolif.* **2025**, *58*, e70033.

[13] Kumar, D.; Gupta, S.; Gupta, V.; Tanwar, R.; Chandel, A. Engineering the future of regenerative medicines in gut health with stem cell-derived intestinal organoids. *Stem Cell Rev. Rep.* **2025**, *21*, 1449–1470.

[14] Petrus-Reurer, S.; Lei, W.; Tysoe, O.; Mairesse, M.; Baez-Ortega, A.; Jones, J.; Tan, T.; Rehakova, S.; Mahbubani, K. T.; Brodie, C. et al. Immunogenicity of autologous and allogeneic human primary cholangiocyte organoid cellular therapies. *Cell Rep. Med.* **2025**, *6*, 102205.

[15] Borges, T. J.; Ganchiku, Y.; Aceves, J. O.; van Gaal, R.; Uzel, S. G. M.; Rosales, I. A.; Rubins, J. E.; Kobayashi, K.; Hiratsuka, K.; Tekguc, M. et al. Exploring immune response toward transplanted human kidney tissues assembled from organoid building blocks. *iScience* **2024**, *27*, 110957.

[16] Chen, S. H.; Saito, Y.; Waki, Y.; Ikemoto, T.; Teraoku, H.; Yamada, S.; Morine, Y.; Shimada, M. Generation of highly functional hepatocyte-like organoids from human adipose-derived mesenchymal stem cells cultured with endothelial cells. *Cells* **2024**, *13*, 547.

[17] Zhou, G. Y.; Li, R. Y.; Sheng, S. H.; Huang, J. T.; Zhou, F. J.; Wei, Y.; Liu, H.; Su, J. C. Organoids and organoid extracellular vesicles-based disease treatment strategies. *J. Nanobiotechnol.* **2024**, *22*, 679.

[18] Kwak, S.; Song, C. L.; Lee, J.; Kim, S.; Nam, S.; Park, Y. J.; Lee, J. Development of pluripotent stem cell-derived epidermal organoids that generate effective extracellular vesicles in skin regeneration. *Biomaterials* **2024**, *307*, 122522.

[19] Mathieu, M.; Martin-Jaular, L.; Lavieu, G.; Théry, C. Specificities of secretion and uptake of exosomes and other extracellular vesicles for cell-to-cell communication. *Nat. Cell Biol.* **2019**, *21*, 9–17.

[20] Ma, X. Y.; Liu, B. B.; Fan, L. M.; Liu, Y. Q.; Zhao, Y. G.; Ren, T. B.; Li, Y.; Li, Y. Y. Native and engineered exosomes for inflammatory disease. *Nano Res.* **2023**, *16*, 6991–7006.

[21] Wu, Z. H.; Cai, H. W.; Tian, C. H.; Ao, Z.; Jiang, L.; Guo, F. Exploiting sound for emerging applications of extracellular vesicles. *Nano Res.* **2024**, *17*, 462–475.

[22] Gao, H.; Zeng, Y. X.; Huang, X. N.; Luodan, A.; Liang, Q. L.; Xie, J.; Lin, X.; Gong, J.; Fan, X. T.; Zou, T. et al. Extracellular vesicles from organoid-derived human retinal progenitor cells prevent lipid overload-induced retinal pigment epithelium injury by regulating fatty acid metabolism. *J. Extracell. Vesicles* **2024**, *13*, e12401.

[23] Park, H. S.; Park, J. H.; Oh, M. K.; Yu, K. R. Advancements in 3D bioprinting for precision medicine: Enhancing patient-derived organoids and extracellular vesicle applications in inflammatory diseases. *Int. J. Bioprint.* **2024**, *10*, 4054.

[24] Du, S.; Guan, Y. C.; Xie, A. H.; Yan, Z.; Gao, S. J.; Li, W. R.; Rao, L.; Chen, X. J.; Chen, T. K. Extracellular vesicles: A rising star for therapeutics and drug delivery. *J. Nanobiotechnol.* **2023**, *21*, 231.

[25] Liao, M. R.; Yao, D. H.; Wu, L. F.; Luo, C. D.; Wang, Z. W.; Zhang, J.; Liu, B. Targeting the Warburg effect: A revisited perspective from molecular mechanisms to traditional and innovative therapeutic strategies in cancer. *Acta Pharm. Sin. B* **2024**, *14*, 953–1008.

[26] Zeng, H. F.; Guo, S. S.; Ren, X. C.; Wu, Z. K.; Liu, S. W.; Yao, X. G. Current strategies for exosome cargo loading and targeting delivery. *Cells* **2023**, *12*, 1416.

[27] Liu, H.; Sun, J. R.; Wang, M. K.; Wang, S. C.; Su, J. C.; Xu, C. Intestinal organoids and organoids extracellular vesicles for inflammatory bowel disease treatment. *Chem. Eng. J.* **2023**, *465*, 142842.
[28] Zhao, S.; Fan, H. L.; Yang, S. X.; Xu, C. Y.; Liu, Y. L.; Guo, Y. X.; Yu, Y. Y.; Sun, Y. F.; Li, H. J.; Wang, Y. et al. Artificial cell derived vesicles from Ginsenoside Rg1-primed mesenchymal stromal cells mitigate oxidative stress and DNA damage in myocardial ischemic/reperfusion injury. *Nano Res.* **2025**, *18*, 94907535.
[29] Qi, C. X.; Liu, X. S.; Zhi, D. K.; Tai, Y. F.; Liu, Y. F.; Sun, Q. Q.; Wang, K.; Wang, S. F.; Midgley, A. C.; Kong, D. L. Exosome-mimicking nanovesicles derived from efficacy-potentiated stem cell membrane and secretome for regeneration of injured tissue. *Nano Res.* **2022**, *15*, 1680–1690.
[30] Mun, S. J.; Ryu, J. S.; Lee, M. O.; Son, Y. S.; Oh, S. J.; Cho, H. S.; Son, M. Y.; Kim, D. S.; Kim, S. J.; Yoo, H. J. et al. Generation of expandable human pluripotent stem cell-derived hepatocyte-like liver organoids. *J. Hepatol.* **2019**, *71*, 970–985.
[31] Qian, X. Y.; Jacob, F.; Song, M. M.; Nguyen, H. N.; Song, H. J.; Ming, G. L. Generation of human brain region-specific organoids using a miniaturized spinning bioreactor. *Nat. Protoc.* **2018**, *13*, 565–580.
[32] Hansen, S. L.; Larsen, H. L.; Pikkupeura, L. M.; Maciag, G.; Guiu, J.; Müller, I.; Clement, D. L.; Mueller, C.; Johansen, J. V.; Helin, K. et al. An organoid-based CRISPR-Cas9 screen for regulators of intestinal epithelial maturation and cell fate. *Sci. Adv.* **2023**, *9*, eadg4055.
[33] He, J.; Cui, H. Y.; Shi, X. H.; Jin, Q. Q.; Han, X. M.; Han, T. T.; Peng, J. Y.; Guo, S. W.; Zhang, L.; Zhao, Y. et al. Functional hepatobiliary organoids recapitulate liver development and reveal essential drivers of hepatobiliary cell fate determination. *Life Med.* **2022**, *1*, 345–358.
[34] Liu, C.; Chen, X. C.; Ene, J.; Esmonde, C.; Kanekiyo, T.; Zeng, C. C.; Sun, L.; Li, Y. Engineering extracellular vesicles secreted by human brain organoids with different regional identity. *ACS Appl. Mater. Interfaces* **2025**, *17*, 15145–15162.
[35] Li, Y. T.; Zheng, Z. L.; Kong, X. X.; Wang, Y. R.; Liu, Z. N.; Wang, W.; Hu, H. G.; Xu, F.; Shi, Y. J. Bacteria extracellular vesicles derived from *Lactobacillus reuteri* delivering intrinsic miR-21a-5p to accelerate diabetic wound healing. *Nano Res.* **2025**, *18*, 94908083.
[36] Toledo, B.; Zhu Chen, L.; Paniagua-Sancho, M.; Marchal, J. A.; Perán, M.; Giovannetti, E. Deciphering the performance of macrophages in tumour microenvironment: A call for precision immunotherapy. *J. Hematol. Oncol.* **2024**, *17*, 44.
[37] Wang, X. Y.; Hu, S. Q.; Zhu, D. S.; Li, J. L.; Cheng, K.; Liu, G. Comparison of extruded cell nanovesicles and exosomes in their molecular cargos and regenerative potentials. *Nano Res.* **2023**, *16*, 7248–7259.
[38] Sheng, C. H.; Guo, X. D.; Wan, Z. Q.; Bai, X. Q.; Liu, H.; Zhang, X.; Zhang, P.; Liu, Y. S.; Li, W. Y.; Zhou, Y. S. et al. Exosomes derived from human adipose-derived stem cells ameliorate osteoporosis through miR-335-3p/Aplnr axis. *Nano Res.* **2022**, *15*, 9135–9148.
[39] Liu, H.; Su, J. C. Organoid and organoid extracellular vesicles for osteoporotic fractures therapy: Current status and future perspectives. *Interdiscip. Med.* **2023**, *1*, e20230011.
[40] Quintard, C.; Tubbs, E.; Jonsson, G.; Jiao, J.; Wang, J.; Werschler, N.; Laporte, C.; Pitaval, A.; Bah, T. S.; Pomeranz, G. et al. A microfluidic platform integrating functional vascularized organoids-on-chip. *Nat. Commun.* **2024**, *15*, 1452.
[41] Lawlor, K. T.; Vanslambrouck, J. M.; Higgins, J. W.; Chambon, A.; Bishard, K.; Arndt, D.; Er, P. X.; Wilson, S. B.; Howden, S. E.; Tan, K. S. et al. Cellular extrusion bioprinting improves kidney organoid reproducibility and conformation. *Nat. Mater.* **2021**, *20*, 260–271.
[42] Hofer, M.; Lutolf, M. P. Engineering organoids. *Nat. Rev. Mater.* **2021**, *6*, 402–420.
[43] Gjorevski, N.; Sachs, N.; Manfrin, A.; Giger, S.; Bragina, M. E.; Ordóñez-Morán, P.; Clevers, H.; Lutolf, M. P. Designer matrices for intestinal stem cell and organoid culture. *Nature* **2016**, *539*, 560–564.
[44] Valdoz, J. C.; Franks, N. A.; Cribbs, C. G.; Jacobs, D. J.; Dodson, E. L.; Knight, C. J.; Poulson, P. D.; Garfield, S. R.; Johnson, B. C.; Hemeyer, B. M. et al. Soluble ECM promotes organotypic formation in lung alveolar model. *Biomaterials* **2022**, *283*, 121464.
[45] Price, S.; Bhosle, S.; Gonçalves, E.; Li, X. D.; McClurg, D. P.; Barthorpe, S.; Beck, A.; Hall, C.; Lightfoot, H.; Farrow, L. et al. A suspension technique for efficient large-scale cancer organoid culturing and perturbation screens. *Sci. Rep.* **2022**, *12*, 5571.
[46] Chang, K. C.; Silvestri, F.; Oliphant, M. U. J.; Martinez-Gakidis, M. A.; Orgill, D. P.; Garber, J. E.; Dillon, D. D.; Brugge, J. S. Breast organoid suspension cultures maintain long-term estrogen receptor expression and responsiveness. *Npj Breast Cancer* **2024**, *10*, 107.
[47] Qian, J. Y.; Lu, E. H.; Xiang, H. B.; Ding, P. B.; Wang, Z.; Lin, Z. Y.; Pan, B. L.; Zhang, C.; Zhao, Z. M. GelMA loaded with exosomes from human minor salivary gland organoids enhances wound healing by inducing macrophage polarization. *J. Nanobiotechnol.* **2024**, *22*, 550.
[48] Ye, S. C.; Marsee, A.; van Tienderen, G. S.; Rezaeimoghaddam, M.; Sheikh, H.; Samsom, R. A.; de Koning, E. J. P.; Fuchs, S.; Verstegen, M. M. A.; van der Laan, L. J. W. et al. Accelerated production of human epithelial organoids in a miniaturized spinning bioreactor. *Cell Rep. Methods* **2024**, *4*, 100903.
[49] Licata, J. P.; Schwab, K. H.; Har-El, Y. E.; Gerstenhaber, J. A.; Lelkes, P. I. Bioreactor technologies for enhanced organoid culture. *Int. J. Mol. Sci.* **2023**, *24*, 11427.
[50] Chen, F.; Zhang, K. S.; Wang, M. J.; He, Z. Y.; Yu, B.; Wang, X.; Pan, X. H.; Luo, Y. P.; Xu, S. J.; Lau, J. T. Y. et al. VEGF-FGF signaling activates quiescent CD63$^+$ liver stem cells to proliferate and differentiate. *Adv. Sci.* **2024**, *11*, e2308711.

This is an open access article under the terms of the Creative Commons Attribution 4.0 International License (CC BY 4.0, https://creativecommons.org/licenses/by/4.0/).

© The Author(s) 2026. Published by Tsinghua University Press.